

From Linear Differential Equations to Unitaries: A Moment-Matching Dilation Framework with Near-Optimal Quantum Algorithms

Xiantao Li,
 The Pennsylvania State University,
 Xiantao.Li@psu.edu

Quantum speed-ups for dynamical simulation usually demand *unitary* time-evolution, whereas the large ODE/PDE systems encountered in realistic physical models are generically *non-unitary*. We present a universal *moment-fulfilling* dilation that embeds any linear, non-Hermitian differential equation $\dot{x} = L(t)x$ with the generator $L = -iH + K$ into a strictly unitary evolution on an enlarged Hilbert space:

$$(|l\rangle \otimes I_A) \mathcal{T} e^{-i \int (I_A \otimes H + iF \otimes K) dt} (|r\rangle \otimes I_A) = \mathcal{T} e^{\int L dt},$$

provided the triple $(F, |r\rangle, |l\rangle)$ satisfies the compact moment identities $(l|F^k|r) = 1$ for all $k \geq 0$ in the ancilla space. This algebraic criterion recovers both *Schrödingerization* [Phys. Rev. Lett. **133**, 230602 (2024)] and the linear-combination-of-Hamiltonians (LCHS) scheme [Phys. Rev. Lett. **131**, 150603 (2023)], while also unveiling whole *families* of new dilations built from differential, integral, pseudo-differential, and difference generators. Each family comes with a continuous tuning parameter *and* is closed under similarity transformations that leave the moments invariant, giving rise to an overwhelming landscape of design space that allows quantum dilations to be co-optimized for specific applications, algorithms, and hardware.

As concrete demonstrations, we prove that a simple finite-difference dilation in a finite interval attains near-optimal oracle complexity, and we also construct a Bargmann–Fock dilation for continuous-variable platforms with a single bosonic mode. Numerical experiments on Maxwell viscoelastic wave propagation confirm the accuracy and robustness of the approach.

I. INTRODUCTION

Large-scale simulations based on ordinary and partial differential equations (ODEs/PDEs) are indispensable to modern, computation-driven physical design and prediction. Their principal bottleneck is *dimension*: realistic models easily involve a huge number of coupled degrees of freedom, making further physical refinement prohibitively expensive on classical hardware. One class of differential equations that can be simulated on quantum computers with a promised exponential speedup is the time-dependent Schrödinger equations (TDSEs), for which many efficient algorithms, known as Hamiltonian simulation algorithms, have been developed with optimal scaling in precision and simulation time [12, 32, 34].

Most differential equations of practical interest, however, are *non-unitary*: relaxation, dissipation or gain render the generator L non-Hermitian on its Hilbert space \mathcal{H} . To harness Hamiltonian-simulation techniques, one must therefore *dilate* the flow, i.e. embed it into a larger Hilbert space on which the evolution becomes unitary. A natural starting point is the decomposition $L = -iH + K$ with $H = H^\dagger$ and $K = K^\dagger$. Two pioneering dilations are the Schrödingerization method [21, 22], which uses a warped-phase ancillary coordinate, and the linear combination of Hamiltonian simulations (LCHS) [2], which realizes the propagator as a Fourier integral.

Both schemes deliver an *exact* embedding, and after a suitable numerical discretization, inheriting the exponential speedup in Hilbert-space dimension together with near-optimal scaling in the evolution time and target precision ϵ [1, 20]. Yet they rely on very different ingredients in the implementation. A recent note [15] further points out that Schrödingerization can be interpreted through the lens of the general Sz.-Nagy dilation theorem [37] as a specific realization. The confluence of these rapid developments, and the clear momentum behind their initial applications [6, 14, 17, 18] brings forth three pressing questions into sharp focus: **(1)** *Is there a unifying abstraction that embraces both existing dilations **and** makes explicit the freedom in choosing the ancillary space and its coupling with the system Hilbert space \mathcal{H} ?* **(2)** *Which structural criteria on a dilation guarantee an exact embedding of the non-unitary dynamics?* **(3)** *Can those criteria be leveraged to systematically generate new, tunable families of dilations tailored to specific algorithms and hardware—from digital qubits to continuous-variable photonics and neutral-atom platforms?*

The present work answers all three questions in the affirmative. Specifically, we present a general framework for treating any linear PDE or ODE system with generator $L(t)$, where we first streamline the dilation into

an Encode-Evolve-Evaluate pipeline:

$$\underbrace{(l| \otimes I)}_{\text{Evaluate}} \underbrace{\mathcal{T}e^{\int_0^t (I_A \otimes H(s) + iF \otimes K(s)) ds}}_{\text{Evolve}} \underbrace{(|r) \otimes I}_{\text{Encode}} \longrightarrow \mathcal{T}e^{\int_0^t L(s) ds}$$

where I_A and F act on an ancillary Hilbert space \mathcal{H}_A . F is skew Hermitian, thus making the dilated operator $I_A \otimes H(s) + iF \otimes K(s)$ Hermitian on $\mathcal{H}_A \otimes \mathcal{H}$. Meanwhile $|r\rangle \in \mathbb{X}$ with \mathbb{X} being a larger function space than \mathcal{H}_A , but approximable by \mathcal{H}_A . The notation $|\cdot\rangle$ indicates that the state might not be normalized. Similarly, $(l|$ is a linear functional on \mathbb{X} . This procedure is inspired by the Schrödingerization method—formulated with warped-phase coordinates and a Fourier transform [22] or in the qumode-quadrature basis [19]. By setting up a general framework that does not presuppose a particular ancilla space, we preserve the flexibility to devise alternative dilation schemes, as demonstrated below.

The main contribution of this paper can be summarized as follows

1. We first show that the dilation is exact, provided that the following moment-matching condition is satisfied: $(l|F^k|r) = 1 (k \geq 0)$, thus providing a set of transparent conditions.
2. We demonstrate that the moment framework immediately reproduces the two classical dilations (Schrödingerization and LCHS) and generates many more. We list five of them in Table I. Each of these choices is expressed as a family of moment-fulfilling dilation schemes with a parameter θ to optimize the simulation complexity.

Space \mathcal{H}_A	Dilation operators	Generator F	Right vector $ r\rangle$	Evaluation $(l $
$H^1(0, 1)$	Differential	$\theta(p\partial_p + \frac{1}{2})$	$p^{1/\theta-1/2}$	$(l f = 2^{1/\theta-1/2}f(\frac{1}{2})$
$L^2(\mathbb{R})$	Integral	$(Ff)(p) = \int_{\mathbb{R}} pe^{-\theta p-q }f(q)dq$	$e^{a(\theta)p}$	$(l f = f(0)$
$L^2(\mathbb{R})$	Pseudo-differential	$-i(-\Delta)^\theta$	$e^{i\xi_0 x}, \xi_0 = e^{i\pi/(4\theta)}$	$(l f = f(0)$
\mathcal{B}	Bargmann–Fock	$\theta(a^\dagger - a)$	$\exp\left(\frac{z^2}{2} - \frac{z}{\theta}\right)$	$(l f = f(0)$
ℓ^2	Difference	$(Ff)_n = \theta(f_n - f_{n-1})$	$\{\lambda_\theta^n\}_{n \geq 0}, \lambda = \frac{\theta}{1+\theta}$	$(l f = f_0$

TABLE I. New one-parameter families of exact moment-dilations. The free parameter θ tunes both the ancillary generator F and the vector $|r\rangle$; the moment conditions Eq. (6) are satisfied in every case.

3. We analyze the dilation scheme based on the differential operator on a compact domain $F = (p\partial_p + \frac{1}{2})$ on $(0, 1)$. Using simple finite-difference discretizations, we show how near-optimal quantum complexity can be easily achieved.
4. Using $F = a^\dagger - a$, we also construct the $(l|$ and $|r\rangle$ pair that fulfills the moment conditions. By working with Bargmann–Fock space, we demonstrate the feasibility of the dilation scheme for continuous variable quantum computing platforms.

A direct consequence of our general dilation scheme is a *universal approximation property* for solution trajectories of arbitrary linear ODEs. Specifically, for any linear PDE/ODE $\dot{\mathbf{x}}(t) = L(t)\mathbf{x}(t)$ and any horizon $T > 0$, there exist a unitary flow $U(t)$ on a dilated Hilbert space and fixed boundary vectors $\langle l|, |r\rangle$ such that $(\langle l| \otimes I)U(t)(|r\rangle \otimes \mathbf{x}_0)$ approximates $\mathbf{x}(t)$ uniformly on $[0, T]$ to arbitrary accuracy. This is achieved by selecting a sequence $|r^{(n)}\rangle \in \mathcal{H}_A$ converging to the target continuous profile and the corresponding duals $\langle l^{(n)}|$, so that the projected unitary trajectories converge to the ODE solution. Notably, the construction is agnostic to spectral or contractive properties of $L(t)$: it applies equally to dissipative, conservative, and transiently or persistently unstable dynamics.

The framework thus bridges current algorithms, offers a catalogue of ready-to-use dilation, and suggests many more yet to be explored by the quantum-algorithm community. Notably, beyond dilation schemes, most of the quantum algorithms have been based on quantum linear solvers [3–5, 8, 10, 24, 41], which also produces a quantum state proportional to the solution $\mathbf{x}(T)$, but requires significantly more state preparation of $|\mathbf{x}_0\rangle$.

Dilation schemes can be viewed as a time-marching scheme, but unlike the method [11], which requires frequent amplitude amplification, dilation schemes wrap the dynamics into a unitary one, and the amplitude amplification is only applied at the final time.

As a specific example, we will analyze the dilation scheme based on a differential operator, which after the spatial discretization, leads to a tight-binding model on the ancilla with nearest-neighbor hoppings. We show that the resulting quantum algorithm exhibits near-optimal complexity in all parameters.

Theorem 1 (Informal main result). *Let $\dot{\mathbf{x}}(t) = (-iH(t) + K(t))\mathbf{x}(t)$ with $H(t) = H(t)^\dagger$ and $K(t) = K(t)^\dagger$ (allowing gain). Using the differential generator $F = p\partial_p + \frac{1}{2}$ and a moment-matching ancilla triple $(F, |r\rangle, \langle l|)$, we construct an exact unitary dilation $\tilde{H}(t) = I_A \otimes H(t) + i\theta F \otimes K(t)$ whose ancilla readout recovers $\mathbf{x}(t)$. After discretization, F becomes a nearest-neighbor tight-binding chain F_h , giving a 2-local qubit implementation and a light-cone suppression of boundary error. With a segment-wise evolution and oblivious amplitude amplification, this yields a near-optimal query complexity $\tilde{\mathcal{O}}(T(H_{\max} + K_{\max}) \|\mathbf{x}(0)\|/\|\mathbf{x}(T)\|)$ (up to standard polylog factors). In the autonomous case ($H(t) \equiv H$, $K(t) \equiv K$), combining segmentation with optimal Hamiltonian simulation yields only an additive logarithmic dependence on precision (of size $\mathcal{O}(\|K\|T \log(\|K\|T/\epsilon))$), and recovers the optimal Hamiltonian-simulation scaling as $\|K\| \rightarrow 0$.*

The remainder of the paper is organized as follows. In Section II we introduce the general moment-fulfilling dilation framework and survey the broad landscape of admissible triples $(F, |r\rangle, \langle l|)$. Section III specializes the framework to a finite-interval, finite-difference dilation that attains nearly optimal scaling in the precision ϵ , evolution time T , and oracle queries to $L(t)$; the section concludes with a numerical demonstration on Maxwell viscoelastic waves. Finally, Section IV presents a Bargmann–Fock realization, showcasing that the scheme is amenable to continuous-variable quantum hardware.

II. PROBLEM SETUP AND MATHEMATICAL FRAMEWORK

We want to simulate the linear systems of N -dimensional ordinary differential equations, or partial differential equations after spatial discretization,

$$\frac{d}{dt}\mathbf{x}(t) = L(t)\mathbf{x}(t), \mathbf{x}(0) = \mathbf{x}_0 \in \mathbb{C}^N. \quad (1)$$

Here $L \in \mathbb{C}^{N \times N}$. Due to the linearity, one can assume that $\|\mathbf{x}_0\| = 1$ without loss of generality. The goal of a differential equation solver is to approximate $\mathbf{x}(t) = \mathcal{T}e^{\int_0^t L(s)ds}\mathbf{x}_0$.

Similar to [2, 21, 22], our approach begins with a partition of L

$$L = -iH + K, \quad (2)$$

with Hermitian matrices H and K . Due to the matrix K , the dynamics of Eq. (1) is non-unitary, which can not be directly treated with Hamiltonian simulation techniques.

We focus on dilation approaches that turn (1) into a Schrödinger equation on an enlarged Hilbert space and is organized in three, as an **E–E–E** pipeline (Encode → Evolve → Evaluate):

1. an **Encoding** step that maps the initial condition in Eq. (1) to a quantum state: $|\Psi(0)\rangle = |r\rangle|\mathbf{x}_0\rangle$. Here we use the notation $|r\rangle$ to highlight a vector that is not in the Hilbert space.

2. an **Evolving** step, where we simulate a unitary dynamics

$$|\Psi(t)\rangle = \mathcal{T}e^{-i\int_0^t \tilde{H}(s)ds} |\Psi(0)\rangle, \quad (3)$$

with a dilated Hamiltonian,

$$\tilde{H}(t) := I_A \otimes H(t) + iF \otimes K(t), \quad (4)$$

with some appropriate skew-Hermitian operator F in a Hilbert space \mathcal{H}_A .

3. an **Evaluating** step that recovers the solution of the original non-unitary dynamics in Eq. (1): $\mathbf{x}(t) = \langle l| \otimes I |\Psi(t)\rangle$, with a suitable linear functional $\langle l|$.

These three steps can be concisely summarized in the following identity,

$$\mathcal{T}e^{\int_0^t L(s)ds} = ((l| \otimes I) \mathcal{T}e^{-i \int_0^t \tilde{H}(s)ds} (|r) \otimes I), \quad \forall t \geq 0. \quad (5)$$

Here I is the identity operator on the original space \mathcal{H} .

To formulate a route that *exactly* embeds the non-unitary dynamics into the unitary dynamics Eq. (3), it is necessary to place it into an infinite-dimensional function space. Specifically, we let \mathbb{X} be a metric function space with $|r) \in \mathbb{X}$, and we let \mathcal{H}_A be the ancilla Hilbert space: $F \in \mathcal{H}$. We require that $\mathcal{H}_A \subset \mathbb{X}$ but \mathcal{H}_A is dense in \mathbb{X} so that F can be extended to functions in \mathbb{X} . Finally, $(l|$ is a linear functional on \mathbb{X} .

Theorem 2 (Moment-fulfilling and Exact Dilation). *Let $L(t) = -iH(t) + K(t)$ be split as in Eq. (2). Then the dilated evolution and recovery exactly reproduces the physical solution as in (5), provided that the following moment conditions are fulfilled,*

$$(l|F^k|r) = 1, \quad \forall k \geq 0. \quad (6)$$

Proof. For autonomous ODEs, A is time-independent. We can express the exponential as a Taylor series, each term can be expanded with powers: $(I_A \otimes H + iF \otimes K)^k$. When taking the moments of each term, $(l|$ and $|r)$ will only act on F , which then is reduced to the Taylor expansion of the matrix exponential of $-iH + K$, and thus completes the proof.

To prove the time-dependent case, we can resort to the time-ordered evolution operator, which involves the time-ordered integrals of the following form,

$$(l|(I_A \otimes H(t_1) + iF \otimes K(t_1))(I_A \otimes H(t_2) + iF \otimes K(t_2)) \cdots (I_A \otimes H(t_k) + iF \otimes K(t_k))|r).$$

Multiplying the operators and using the fact that $(l|I_A|r) = 1$ and the properties in Eq. (6), we find that the product is reduced to,

$$(H(t_1) + iK(t_1))(H(t_2) + iK(t_2)) \cdots (H(t_k) + iK(t_k)),$$

leading exactly to the Dyson series expansion for the time-ordered evolution operator associated with $L(t)$. \square

It is crucial to point out that working entirely in a Hilbert space will never fulfill the moment conditions Eq. (6). If both $(l|, |r) \in \mathcal{H}_A$, then one can see the following contradiction: the right hand side of Eq. (5) is bounded for all t , whereas the left hand side has no such guarantee. It is precisely this use of states outside the ancilla Hilbert space that grants the dilation its power. One important implication of the current result is that the trajectories from (5) are dense in the solution space of any linear ODE system, including those with transient or persistent solution growth, thus achieving a theoretical universal approximation theorem using time-dependent Schrödinger equations. This can be seen by choosing an approximation of $|r)$ in \mathcal{H} , with which the dynamics generated by $\tilde{H}(t)$ is unitary.

A simple recipe to fulfill the moment conditions Eq. (6) is to ensure $F|r) = |r)$ and $(l|r) = 1$. Since F is skew Hermitian, and thus has purely imaginary eigenvalues in the Hilbert space \mathcal{H}_A , it is again necessary that $|r)$ is an eigenfunction outside \mathcal{H}_A .

Corollary 1. *The moment conditions (6) are invariant under any similarity transformation. Namely, for any invertible map S , $(l|S^{-1}, SFS^{-1}$ and $S|r)$ also fulfill the moment conditions, and thus lead to exact dilations as well. By choosing S to be a unitary operator, SFS^{-1} remains skew Hermitian.*

In addition to the variations of the exact dilation scheme with similarity transformations, we will show five examples below, and two more examples in the next section.

Example 1 (Schrödingerization via warped-phase transformation [22]). *The Schrödingerisation approach can be associated with an ancillary Hilbert space.*

$$\mathcal{H}_A = \{f, f' \in L^2((0, \infty), dp) \mid f(0) = 0\},$$

with inner product $\langle f, g \rangle := \int_0^\infty f(p)^* g(p) dp$. In addition, the triple is selected as follows,

$$F := -\frac{d}{dp}, \quad |r) = e^{-p}, \quad (l|f(p) \mapsto e^{p^*} f(p^*). \quad (7)$$

Here $p^* > 0$ is arbitrary. Another choice of the evaluation is $(l|f(p) \mapsto \int_0^{+\infty} f(p)dp)$ [18]. It is clear that $|r| \notin \mathcal{H}_A$, due to the violation of the boundary condition. In this case, the function space \mathbb{X} can be chosen to be $C_0(0, \infty)$ to contain $|r|$. In addition, simple calculations verify that the exact moment conditions $(l|F^k|r) = 1, k = 0, 1, 2, \dots$ are fulfilled.

Example 2 (Linear combination Hamiltonian simulations (LCHS) [2]). LCHS expresses the solution of Eq. (1) as an integral with the Lorentzian kernel. To put it into the framework of (5), we can choose the ancillary Hilbert space to be the real Schwartz class endowed with the usual L^2 inner product,

$$\mathcal{H}_A = \mathcal{S}(\mathbb{R}), \quad \langle f, g \rangle = \int_{-\infty}^{\infty} f(k)^* g(k) dk.$$

Multiplication by ik leaves \mathcal{H}_A invariant, hence we may take the skew-Hermitian ancillary generator $F = ik$. In addition, we set

$$|r|(k) = \frac{-i}{k - i}, \quad (l|f = \frac{i}{\pi} \int_{-\infty}^{\infty} \frac{f(k)}{k + i} dk,$$

thus giving the LCHS formula,

$$\mathcal{T} e^{\int_0^t L(s) ds} = \frac{1}{\pi} \int_{\mathbb{R}} \mathcal{T} e^{-i \int_0^t H(s) + k K(s) ds} \frac{1}{k^2 + 1} dk.$$

Although $|r| \notin \mathcal{S}$, it still decays algebraically and it can be contained in the tempered-distribution space $\mathbb{X} := \mathcal{S}'(\mathbb{R})$. The moment condition Eq. (6) is then interpreted via contour integrals in the complex k -plane (with contributions from the simple poles at $k = i$) and can be verified using Cauchy's residue theorem. LCHS has been improved to near-optimal query complexity [1, 16, 33, 39] and extended to infinite dimensions [35].

The LCHS has an interesting connection to the Schrödingerization method in the previous example. Let \mathcal{F} denote Fourier transform, one can apply the inverse Fourier transform to the triple, and restrict to the half-line $p > 0$: $(\mathcal{F}^{-1}|r|)(p) = e^{-p} 1_{(0, \infty)}(p)$. Similarly, one can show that $\mathcal{F}^{-1} \circ F \circ \mathcal{F} = -\frac{d}{dp}$, and $(l|\mathcal{F}f = e^{p^*} f(p^*)$. Thus in the dual p -representation the triple coincides with the warped-phase Schrödingerization example.

Another natural choice for constructing a Hilbert space is by using integral operators.

Example 3 (Integral-kernel dilation). For a scale $\theta > 0$ define the odd kernel $K_\theta(p) = pe^{-\theta|p|}$. Its convolution $(F_\theta f)(p) = \int_{\mathbb{R}} K_\theta(p - q) f(q) dq$ is skew-Hermitian on $\mathcal{H}_A = L^2(\mathbb{R})$. Meanwhile, for $a \in (-\theta, 0)$ one finds $F_\theta e^{ax} = \lambda_\theta(a) e^{ax}$, $\lambda_\theta(a) = -4\theta a / (\theta^2 - a^2)^2$. Choosing a so that $\lambda_\theta(a) = 1$ (e.g. $\theta = 1 \Rightarrow a \approx -0.2253$) gives

$$|r\rangle(x) = e^{ax}, \quad F_\theta|r\rangle = |r\rangle.$$

By taking $\langle l|f = f(0)$, the moment identities are exactly satisfied.

Although $|r| \notin \mathcal{H}_A$, it lies in the weighted space $\mathbb{X} = L^2(e^{-2\gamma|x|}, dx)$ for any $\gamma \in (-a, \theta)$, where \mathcal{H}_A is dense. Discretising F via Nyström quadrature yields a narrow-band matrix that might be amenable to block-encoding.

Another convenient way to generate skew operators is through pseudodifferential symbols $a(x, \xi)$:

$$(\text{Op}(a)f)(x) = \frac{1}{2\pi} \int_{\mathbb{R}} \int_{\mathbb{R}} e^{i(x-y)\xi} a(x, \xi) f(y) dy d\xi.$$

Example 4 (Dilation via a pseudodifferential generator). Let the ancillary Hilbert space be $\mathcal{H}_A = L^2(\mathbb{R}, dx)$. Fix an order $0 < \theta \leq 1$ and define the pseudodifferential generator

$$F := -i(-\Delta)^\theta, \quad [(\widehat{-\Delta}^\theta f)](\xi) = (\xi^2)^\theta \hat{f}(\xi).$$

Because $(-\Delta)^\theta$ is self-adjoint and positive, the factor $-i$ makes F skew-Hermitian on \mathcal{H}_A . A natural choice for $|r|$ is the plane wave $|r\rangle(x) = e^{i\xi_0 x}$, with a complex frequency ξ_0 so that $|r| \notin \mathcal{H}_A$ and the evaluation functional $\langle l|f = f(0)$. By choosing ξ_0 such that $\xi_0^{2\theta} = i$, we have $F|r\rangle = -i\xi_0^{2\theta} |r\rangle = |r\rangle$. Thus all the moment conditions in Eq. (6) are satisfied. Selecting $\arg(\xi_0^2) = \pi/2$ then forces $(\xi_0^2)^\theta = e^{i\pi/2} = i$, i.e., $\xi_0 = e^{i\pi/(4\theta)}$ from the principal branch.

Example 5 (Dilations using difference operators). *Consider a class of difference operators, applied to the space of infinite sequences $\mathcal{H}_A = \ell^2$, with each $f \in \ell^2$ being $f = (0, f_1, \dots)$ equipped with the inner product: $\langle f, g \rangle = \sum_{n \geq 1} f_n^* g_n$. We can define a difference operator θF as, $(\theta F f)_0 = 0$ and $(\theta F f)_n = \theta(f_n - f_{n-1})$ when $n \geq 1$. A telescopic (summation-by-parts) calculation gives $F_\theta^\dagger = -F_\theta$ on \mathcal{H}_A . In addition, one can verify that with $|r\rangle = \{\lambda_\theta^n\}_{n \geq 0}$, $\lambda_\theta = \frac{\theta}{1+\theta} \in (0, 1)$, and $(l|f = f_0$ or $(l|f = \lambda_\theta^{-1} f_1$ the moment conditions (6) are satisfied.*

These examples show the overwhelming possibilities of achieving the exact dilations, in addition to the dilation scheme created by a similarity transformation among $(l|$, F , and $|r\rangle$. This wide variety of such dilation methods forms a large platform where different quantum algorithms can be invoked. For example, the dilated Hamiltonian in Example 4 and Example 3 might be efficiently implemented using the block-encoding techniques in [27, 38].

In the next two sections, we will closely examine two approaches, one based on a first-order differential equation, for which a finite-difference approximation leads to simple implementation on digital quantum computers, the other based on Bargman representation of a boson environment [13], which is more suited for continuous variable quantum platforms.

III. A DILATION USING A FUNCTION SPACE ON A COMPACT DOMAIN

The five examples in the previous section work with an ancilla Hilbert space in \mathbb{R} , \mathbb{R}_+ or \mathbb{N} , forcing one to truncate tails in a numerical implementation, thus introducing additional complications. Here we present a model whose dilation acts on a *finite* interval, so the dilation operator can be made uniformly banded for which the algorithmic complexity is easy to control.

A. Numerical discretizations using SBP

To find a dilation in Eq. (5), we let

$$\mathcal{H}_A := H_0^1(0, 1) = \{f \in L^2(0, 1) \mid f' \in L^2(0, 1), f(1) = 0\}, \quad \langle f, g \rangle = \int_0^1 f(p)^* g(p) dp.$$

Define the generator as the differential operator $F_\theta = \theta F$, and

$$F := p\partial_p + \frac{1}{2}. \quad (8)$$

Lemma 1. *For every $\theta > 0$ the operator θF is skew-Hermitian on \mathcal{H}_A . Moreover, the moment conditions of (6) are satisfied with*

$$|r\rangle = p^\beta, \quad (l|f = 2^\beta f\left(\frac{1}{2}\right),$$

where the exponent β is

$$\beta = \frac{1}{\theta} - \frac{1}{2}. \quad (9)$$

Proof. Skewness: for $f, g \in \mathcal{H}_A$, we examine the inner product denoted by $\langle \cdot, \cdot \rangle$,

$$\langle f, Fg \rangle = \int_0^1 f^*(pg' + \frac{1}{2}g) dp = pf^*g\Big|_0^1 - \langle Ff, g \rangle, \quad (10)$$

and the boundary term vanishes since $p = 0$ at the left endpoint and $f(1) = g(1) = 0$ at $p = 1$. Hence F is skew-Hermitian and so is θF . For the moments, $F(p^\beta) = (\beta + \frac{1}{2})p^\beta$; with (9) we get $F_\theta|r\rangle = \theta(\beta + \frac{1}{2})|r\rangle = |r\rangle$. Also, $\langle l|r\rangle = 2^\beta r(1/2) = 2^\beta \cdot 2^{-\beta} = 1$. \square

Note $|r\rangle \notin H_0^1$ only because it fails the condition $r(1) = 0$, but $r \in C^1(0, 1)$ and $r \in H^1(0, 1)$ since $\beta > 1/2$ when $\theta \in (0, 1)$, so the dilation remains well-posed.

For a qubit implementation, we discretize $\{F, \langle l |, |r \rangle\}$ as follows. Partition $[0, 1]$ into M intervals with grid points $\{p_i\}_{i=0}^M$ and set $v_i = v(p_i)$. The integration by parts that ensured the skew Hermitian property can be extended to the discrete level using summation by parts (SBP). Following [36, 40], we let $h_j := p_{j+1} - p_j$ and define the SBP trapezoid weights

$$W = \text{diag}(w_0, \dots, w_M), \quad w_0 = \frac{1}{2}h_0, \quad w_j = \frac{1}{2}(h_{j-1} + h_j) \ (1 \leq j \leq M-1), \quad w_M = \frac{1}{2}h_{M-1}. \quad (11)$$

Let Q be the tridiagonal matrix with

$$(Q)_{j,j+1} = \frac{1}{2}, \quad (Q)_{j+1,j} = -\frac{1}{2}, \quad Q_{00} = -\frac{1}{2}, \quad Q_{MM} = +\frac{1}{2}, \quad (12)$$

and set $D := W^{-1}Q$. Then the diagonal-norm SBP identity holds:

$$WD + D^\dagger W = Q + Q^\dagger = B := \text{diag}(-1, 0, \dots, 0, 1).$$

This implies that for all grid functions \mathbf{u}, \mathbf{v} , $\langle \mathbf{u}, D\mathbf{v} \rangle_W + \langle D\mathbf{u}, \mathbf{v} \rangle_W = u_M v_M - u_0 v_0$ with weighted inner product $\langle \mathbf{x}, \mathbf{y} \rangle_W := \mathbf{x}^\dagger W \mathbf{y}$, thus mimicking the integration by parts property in Eq. (10), and thus automatically maintain the skew property after the discretization. Specifically, let $P := \text{diag}(p_0, \dots, p_M)$ and define the (Hamiltonian) split form

$$F_w := \frac{1}{2}(PD + DP) - \frac{1}{2}W^{-1}BP, \quad F_h := W^{1/2}F_wW^{-1/2}. \quad (13)$$

The SBP property automatically guarantees that F_h is skew-Hermitian and tridiagonal, while F_w is skew with respect to the W -inner product. On a uniform grid one has $h_i \equiv h := 1/M$, $p_i = ih$, $i = 0, \dots, M$, and $w_0 = w_M = h/2$, $w_i = h$, $\forall 1 \leq i \leq M-1$. The second-order SBP approximation of F in Eq. (8) reads

$$\begin{aligned} (F_h v)_0 &= \frac{1}{2\sqrt{2}}v_1, \\ (F_h v)_1 &= \frac{3}{4}v_2 - \frac{1}{2\sqrt{2}}v_0, \\ (F_h v)_i &= \frac{p_{i+1}+p_i}{4h}v_{i+1} - \frac{p_i+p_{i-1}}{4h}v_{i-1}, \quad 2 \leq i \leq M-1, \\ (F_h v)_M &= -\frac{p_{M-1}+p_M}{4h}v_{M-1}. \end{aligned} \quad (14)$$

The skew-Hermitian property is apparent.

With the approximation of F by $F_h \in \mathbb{C}^{(M+1) \times (M+1)}$, we obtain a dilated Hamiltonian,

$$\tilde{H}(t) := I \otimes H(t) + i\theta F_h \otimes K(t). \quad (15)$$

The implementation of $\tilde{H}(t)$ requires an appropriate representation of F_h on quantum devices. The SBP split form can be written as $F_h = a - a^\dagger$, where $a := \sum_{j=0}^{M-1} f_j |j\rangle\langle j+1|$ is a weighted lowering operator. In this sense iF_h plays the role of a discrete momentum/current operator on a tight-binding chain (a discrete derivative up to constants). With $|r_h\rangle = W^{1/2}\mathbf{1}$, the right vector is the mass-weighted flat mode: for $\theta = 2$, the SBP closure gives $\theta F_h |r_h\rangle = |r_h\rangle$ on all interior sites.

We can also associate F_h with Pauli strings, which provide more alternatives to the implementation on digital quantum computers. Using a unary (one-hot) encoding of the ancilla with computational basis $|j\rangle_{j=0}^M$, define $\sigma_j^\pm = (X_j \mp iY_j)/2$. For the off-diagonal couplings f_j , the split-form chain satisfies $(F_h)_{j,j+1} = f_j$, $(F_h)_{j+1,j} = -f_j$, hence $(iF_h)_{j,j+1} = if_j$, $(iF_h)_{j+1,j} = -if_j$. It admits the 2-local Pauli expansion

$$F_h = \sum_{j=0}^{M-1} f_j (\sigma_j^+ \sigma_{j+1}^- - \sigma_j^- \sigma_{j+1}^+), \implies iF_h = -\frac{1}{2} \sum_{j=0}^{M-1} f_j (X_j Y_{j+1} - Y_j X_{j+1}).$$

Meanwhile, for the initial state $|r\rangle$ (an eigenvector of F), we take the direct discretization with normalizing factor Z_β ,

$$|r_h\rangle = |r_h\rangle = Z_\beta^{-1} \sum_{j=0}^M p_j^\beta w_j^{1/2} |j\rangle, \quad Z_\beta = \left(\sum_{j=0}^M w_j p_j^{2\beta} \right)^{1/2} = \mathcal{O}\left(\frac{1}{\sqrt{2\beta+1}}\right). \quad (16)$$

Take $(l_h| = \frac{1}{\langle j_* | r_h \rangle} \langle j_* |$, for some $0 \leq j_* < M$. Then $(l_h | r_h) = 1$ by construction.

These elements constitute a simple procedure to simulate the ODEs (1): Starting with $|r_h\rangle \otimes |\mathbf{x}_0\rangle$, one applies Hamiltonian simulations with the dilated Hamiltonian (15) to time T , and then post-select at j_* on the ancilla. In the following sections, we will analyze the error due to the discretization and the success probability from the post-selection.

B. Error Estimation using a Light-cone Property

Considering the simple choice $\beta = 0$, i.e., $\theta = 2$, then $|r_h\rangle = \sqrt{h/2}|0\rangle + \sqrt{h}|1\rangle + \cdots + \sqrt{h}|M-1\rangle + \sqrt{h/2}|M\rangle$. A direct calculation shows that $\langle j | \theta F_h | r_h \rangle = \langle j | r_h \rangle$ for all $j < M$, which is guaranteed by the SBP construction. Similarly, $\langle j | (\theta F_h)^2 | r_h \rangle = \langle j | r_h \rangle$ for all $j < M-1$. Therefore,

$$(l_h | (\theta F_h)^k | r_h) = 1, \forall k < M - j_*, \quad (17)$$

which is an indication of the approximate property via a finite moment matching of (6).

One remarkable observation is that by adding one diagonal entry to F_h ,

$$\widehat{F}_h = F_h + \alpha |M\rangle\langle M|, \quad \alpha = \frac{1}{\theta} - \frac{\langle M | F_h | r_h \rangle}{\langle M | r_h \rangle} = \mathcal{O}(M). \quad (18)$$

we obtain $\theta \widehat{F}_h | r_h \rangle = | r_h \rangle$, implying that the triple $\langle l_h |, \widehat{F}_h, | r_h \rangle$ satisfies moment conditions of *all orders* with a finite-dimensional, almost skew-Hermitian operator \widehat{F}_h . In light of Theorem 2, the dilation using a finite-dimensional non-Hermitian \widehat{F}_h recovers the exact solution of the ODEs (1). We will refer to such correction as moment-locking closure (MLC).

The benefit of MLC is two-fold. First, using \widehat{F}_h provides a simple route to quantify the error by the dilated Hamiltonian without going to infinite dimensions. Although \widehat{F}_h is non-Hermitian, it provides an analysis device to quantify the error. Secondly, compared to the infinite-dimensional formulae, such as Schrödingerization [22], LCHS [2], and (5), it provides an easier starting point to design successively improved approximations.

To elaborate on the first point, we also define $\widehat{H}(t) := I \otimes H(t) + i\theta \widehat{F}_h \otimes K(t)$, along with the dynamics they generate,

$$i \frac{d}{dt} \Psi(t) = \widetilde{H}(t) \Psi(t), \quad \Psi(0) = |r_h\rangle \otimes \mathbf{x}_0, \quad (19)$$

$$i \frac{d}{dt} \Phi(t) = \widehat{H}(t) \Phi(t), \quad \Phi(0) = |r_h\rangle \otimes \mathbf{x}_0. \quad (20)$$

Since $\theta \widehat{F}_h$ has $|r_h\rangle$ as an eigenvector with eigenvalue 1, $\Phi(t) = |r_h\rangle \otimes \mathbf{x}(t)$. Define the error $\chi(t) := \Phi(t) - \Psi(t)$. Subtracting the two evolutions yields

$$i \frac{d}{dt} \chi(t) = \widetilde{H}(t) \chi(t) + i\theta \alpha (|M\rangle\langle M| \otimes K(t)) \Phi(t), \quad \chi(0) = 0.$$

In the error equation, the source of the error clearly concentrates at the right boundary only in the ancilla. Since F_h in \widetilde{H} only has nonzero entries at off-diagonals $(j, j+1)$ and $(j+1, j)$, the error propagation to the left, especially the arrival at j_* , where we post-select the solution, can be estimated by a light-cone type of approach [29], which in the context of the differential operator in Eq. (8), is known as the CFL condition [26]. Fig. 1 shows a numerical demonstration of such back propagation of the boundary error using the ODE $\frac{d}{dt} \mathbf{v} = -\theta \kappa(t) F_h \mathbf{v}$, where one sees the boundary perturbation confined to the characteristic cone emanating from $p = 1$ with speed $-\theta p$; points outside that domain of dependence remain unchanged. The arrival time at a location p_* scales like

$$T(1 \rightarrow p_*) = -\ln p_*. \quad (21)$$

See Section A and Lemma 5 for a derivation. We now quantify such error propagation.

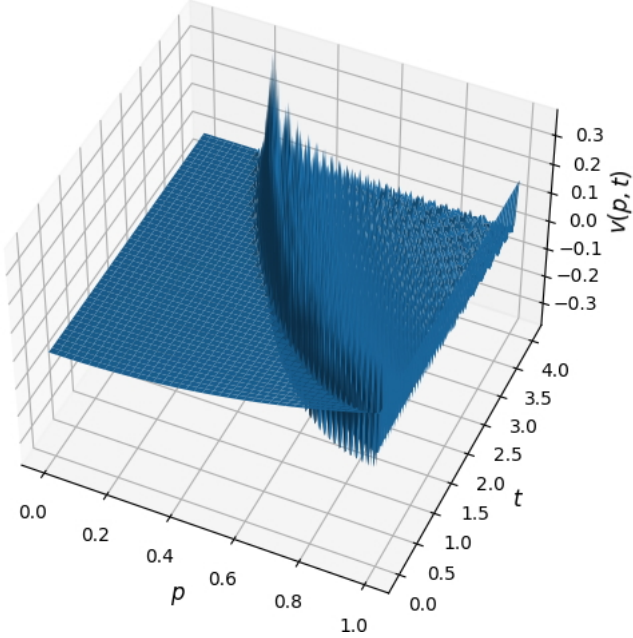


FIG. 1. Snapshots of the semi-discrete solution for $\mathbf{v}' = -\theta F_h \mathbf{v}$ with $v_j(0) \propto p_j^{1/\theta-1/2}$.

Lemma 2 (Finite-speed propagation bound). *Let $\theta = 2$ and consider the uniform grid with grid size $h = 1/M$. Suppose $m = M - j_*$ and that*

$$\varrho := \frac{2e\theta K_{\max}T}{mh} < \frac{1}{2}, \quad (22)$$

then the boundary-induced error arriving at $p_ = j_*h$ obeys*

$$\|(\langle j_* | \otimes I)\chi(T)\| \leq 2\alpha |\langle M | r_h \rangle| X(T) K_{\max} T \left(\frac{1}{2}\right)^{M-j_*}, \quad X(T) := \sup_{t \in [0, T]} \|\mathbf{x}(t)\|. \quad (23)$$

Consequently, to guarantee $\|(\langle j_ | \otimes I)\chi(T)\| \leq \epsilon$, it suffices to choose*

$$M - j_* \geq \log_2 \frac{4\alpha X(T) K_{\max} T}{\epsilon}. \quad (24)$$

As a result, under the condition in Eq. (22), especially when $K_{\max}T = \mathcal{O}(1)$ we can make the geometric factor smaller than ϵ by taking $M = \Omega(\log(K_{\max}TX(T)/\epsilon))$ (Thus the number of ancilla has $\log \log(K_{\max}TX(T)/\epsilon)$ scaling). Since F_h is 2-sparse and $\|F_h\|_2 = \Theta(1/h) = \Theta(M)$, by using the matrix norm bounds for sparse matrices, the dilated Hamiltonian (15) obeys

$$\|\tilde{H}(t)\| = \mathcal{O}(H_{\max} + \theta K_{\max} M) = \mathcal{O}\left(H_{\max} + \theta K_{\max} \log \frac{K_{\max} TX(T)}{\epsilon}\right),$$

where $H_{\max} := \max_{0 \leq t \leq T} \|H(t)\|$. Leveraging the time-dependent Hamiltonian simulations using Dyson series [34], we arrive at,

Theorem 3 (ODE simulations by dilation under the light-cone condition (22)). *Assume that $K_{\max}T = \mathcal{O}(1)$, and assume block encodings of $H(t)$ and $K(t)$ with norms H_{\max} and K_{\max} , respectively. The dilation scheme outputs an ϵ -accurate approximate state for $|\mathbf{x}(t)\rangle$ with success probability $\Omega(1)$ using*

$$\tilde{\mathcal{O}}\left(\frac{(TH_{\max} + \log \frac{X(T)}{\epsilon})\|\mathbf{x}(0)\|}{\|\mathbf{x}(T)\|}\right)$$

block-encoding queries to $H(t)$ and $K(t)$, and a comparable number of gates, where $\tilde{\mathcal{O}}$ hides the $\frac{\log TH_{\max}/\epsilon}{\log \log TH_{\max}/\epsilon}$ factor. For autonomous ODEs where $K(t)$ and $H(t)$ are time-independent, the query complexity is reduced to,

$$\mathcal{O} \left((TH_{\max} + \log \frac{X(T)}{\epsilon} + \log \frac{TH_{\max}}{\epsilon}) \frac{\|\mathbf{x}(0)\|}{\|\mathbf{x}(T)\|} \right).$$

C. Geometrically refined grids with an improved light-cone property

The arrival-time estimate based on the PDEs generated by F suggests that the propagation of the boundary effect slows down when it is approaching the left boundary $-\log p_*$. This suggests that we mitigate a large $K_{\max}T$ by refining only near the left boundary while keeping the bulk step size moderate. We therefore adopt a *geometric* grid

$$p_j = \exp \left[-\delta(M-j) \right], \quad j = 0, 1, \dots, M, \quad (25)$$

with grading parameter $\delta > 0$ ($\delta = 1$ is enough for the discussions below). One can directly verify that the (trapezoidal) diagonal quadrature weights are

$$w_j = \begin{cases} \frac{1}{2}(e^\delta - 1)p_0, & j = 0, \\ \frac{p_{j+1} - p_{j-1}}{2} = p_j \sinh \delta, & 1 \leq j \leq M-1, \\ \frac{1}{2}(1 - e^{-\delta})p_M, & j = M, \end{cases}$$

and the split-form skew tridiagonal off-diagonals $f_j := (F_h)_{j,j+1}$ in Eq. (13) are uniform in the interior, which makes it easier to analyze and implement. Specifically, we have,

$$f_j = \frac{1}{4 \sinh(\delta/2)} \times \begin{cases} \sqrt{1 + e^{-\delta}}, & j = 0, \\ 1, & 1 \leq j \leq M-2, \\ \sqrt{1 + e^\delta}, & j = M-1. \end{cases} \quad (26)$$

We consider $\delta \geq \delta_0$ with a constant δ_0 , which implies that,

$$\|F_h\| \leq 2 \max_{0 \leq j \leq M-1} f_j = \frac{\sqrt{1 + e^\delta}}{2 \sinh(\delta/2)} = \Theta(1). \quad (27)$$

We now state the finite-propagation estimate on the geometric chain. The proof is shown in Section A 2.

Lemma 3 (Finite-speed propagation on a geometric chain). *Let F_h be the skew-Hermitian chain with off-diagonals f in (26) and $j_* \in [M-1]$. If*

$$\varrho := \frac{e\theta K_{\max}T}{4(M-j_*) \sinh(\frac{\delta}{2})} < 1, \quad (28)$$

then the boundary influence decays geometrically.

$$\|\langle j_* | \otimes I \chi(T) \| \leq \frac{\varrho^{M-j_*}}{1 - \varrho^2}. \quad (29)$$

The condition in (28) is significantly better than Eq. (22). Choosing $\delta = \Theta(1)$ and $M = \Theta(K_{\max}T)$ is sufficient to make the base $\varrho < 1$, and an additional $\mathcal{O}(\log(1/\epsilon))$ points pushes the error below ϵ . Furthermore, one can choose a much larger δ to enhance this property, e.g., $\delta = \log(K_{\max}T)$. However, the downside of this approach is that the right vector $\langle j | r_h \rangle \propto W_j^{1/2}$ has exponentially small components near the left boundary,

thus leading to a small success probability. On the other hand, by choosing a large post-select window $[0, p_{j_*}]$, the small probability can be improved to $\Omega(1)$, but in this case, Eq. (28) is difficult to satisfy.

So for long-time simulation where $K_{\max}T \gg 1$, we divide the simulation into segments, each with length $\tau \mathcal{O}(1/K_{\max})$. Upon the completion of the Hamiltonian evolution of each segment, one obtains an accurate solution in the window $[0, p_{j_*}]$, thanks to the light-cone condition in Eq. (28). To transition to the next time segment, we simply apply oblivious amplitude amplifications (OAA) to restore the ancilla state back to $|r_h\rangle$.

Corollary 2 (Light-cone protected window with constant weight). *Fix constants $\delta_0 > 0$ and $\Delta \in (0, 1/2)$, and assume $\delta \geq \delta_0$. Let $m := M - j_* \geq 1$ and choose*

$$m \geq \max \left\{ \frac{1}{2 \sinh(\delta/2)}, \frac{1}{\delta} \log \left(\frac{1+e^\delta}{2\Delta} \right) \right\}. \quad (30)$$

If the segment length τ satisfies

$$\tau \leq \frac{1}{e \theta K_{\max}}, \quad (31)$$

then for the readout site $j_* := M - m$ we have:

(i) (Light-cone) the geometric-chain parameter obeys

$$\varrho = \frac{e\theta K_{\max} \tau}{4m \sinh(\delta/2)} \leq \frac{1}{2},$$

so Lemma 3 applies at j_* over time τ ;

(ii) the window probability satisfies

$$P_{\text{win}}(j_*) = \frac{\frac{1}{2}(p_{j_*} + p_{j_*+1}) - p_0}{1 - p_0} \geq \Delta - p_0, \quad p_0 = e^{-\delta M}.$$

Since p_0 is exponentially small with M , we can pick a safe lower bound $\Delta/2$ by choosing a sufficiently large M .

(iii) $\|F_h\| = \mathcal{O}(1)$.

Proof. (i) Using (31) gives

$$\varrho = \frac{e\theta K_{\max} \tau}{4m \sinh(\delta/2)} \leq \frac{1}{4m \sinh(\delta/2)} \leq \frac{1}{2},$$

by the first lower bound in (30).

(ii) With $j_* = M - m$, we have $p_{j_*} = e^{-\delta m}$ and $p_{j_*+1} = e^{-\delta(m-1)}$, hence

$$P_{\text{win}}(j_*) = \frac{\frac{1}{2}(e^{-\delta m} + e^{-\delta(m-1)}) - p_0}{1 - p_0} \geq \frac{1}{2}(e^{-\delta m} + e^{-\delta(m-1)}) - p_0 = \frac{1+e^\delta}{2} e^{-\delta m} - p_0.$$

The second lower bound in (30) ensures $\frac{1+e^\delta}{2} e^{-\delta m} \geq \Delta$, giving the claim.

(iii) This comes directly from the magnitude of f_j 's. □

D. Segmentation-wise simulation and oblivious amplitude amplification

We describe a segmented algorithm for approximating the normalized solution. Specifically, consider a partition $[0, T] = \bigcup_k [t_k, t_{k+1}]$, where $t_k := k\tau$, with τ selected as follows

$$\tau K_{\max} = \mathcal{O}(1). \quad (32)$$

We also let

$$\mathcal{U}_k := \mathcal{T} \exp \left(-i \int_{t_k}^{t_{k+1}} \tilde{H}(s) ds \right) \quad (33)$$

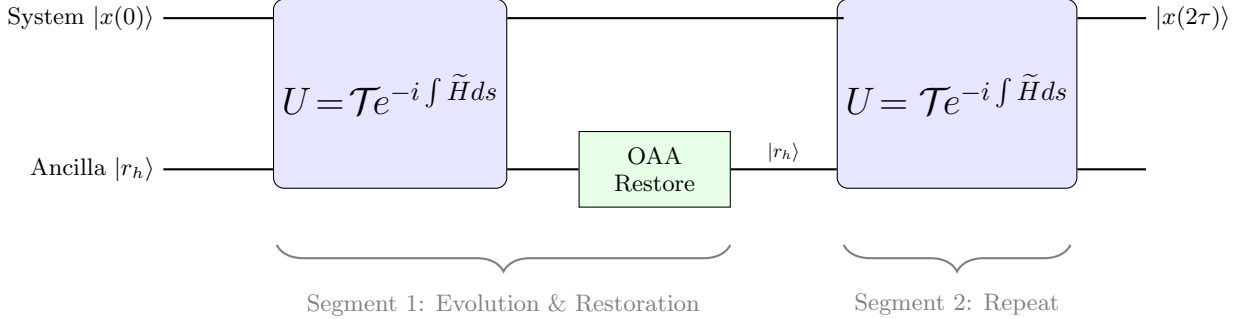


FIG. 2. Circuit diagram for the segmented simulation. The algorithm proceeds in time steps of duration τ . In each segment, the joint evolution $U_k = \mathcal{T} \exp(-i \int \tilde{H} ds)$ is applied. The system state evolves from $|x(t)\rangle$ to $|x(t+\tau)\rangle$ (conditioned on success), while the ancilla is restored to the reference state $|r_h\rangle$ via Oblivious Amplitude Amplification (OAA) before the next segment begins.

be the segment propagator on $[t_k, t_{k+1}]$. After each segment, we restore the ancilla back to $|r_h\rangle$ using OAA. The overall workflow is depicted in Fig. 2.

The light-cone property ensures that the prefront window $\text{win} = \{0, 1, \dots, j_*\}$ on the ancilla lattice is unaffected by the boundary error (up to an ϵ error), and retains the solution $\mathbf{x}(t)$ within the win . In particular, within the choice of Eq. (32) for τ , $P_{\text{win}} := \sum_{j \in \text{win}} |\langle j | r_h \rangle|^2$ is a constant lower bound thanks to Corollary 2, and without loss of generality, we may set $P_{\text{win}} \geq 1/4$. Let us define the corresponding projector and the truncated ancilla mode, respectively,

$$\Pi_{\text{win}} := \left(\sum_{j \in \text{win}} |j\rangle \langle j| \right) \otimes I, \quad |r_{\text{win}}\rangle := \sum_{j \in \text{win}} |j\rangle \langle j | r_h \rangle. \quad (34)$$

Write the (normalized) solution from the previous segment k as $|\Psi_k\rangle$. The post-window state decomposes as

$$\mathcal{U}_k |\Psi_k\rangle = \underbrace{\Pi_{\text{win}} \mathcal{U}_k |\Psi_k\rangle}_{=: |G_k\rangle} + \underbrace{(I - \Pi_{\text{win}}) \mathcal{U}_k |\Psi_k\rangle}_{=: |B_k\rangle}, \quad \langle G_k | B_k \rangle = 0. \quad (35)$$

The success probability of a direct window postselection is $p_k := \| |G_k\rangle \|^2$.

Since the boundary-induced component that reaches the window win during a single segment is exponentially small, there exists an error vector $|\mathbf{e}_k\rangle$ supported on win such that

$$\Pi_{\text{win}} \mathcal{U}_k |\Psi_k\rangle = |r_{\text{win}}\rangle \otimes |\mathbf{x}(t_{k+1})\rangle + |\mathbf{e}_k\rangle, \quad \|\mathbf{e}_k\| \leq \epsilon. \quad (36)$$

Equation (36) formalizes an important observation that the unwanted boundary disturbance has *negligible overlap* with the “good” component supported on the window win , and one can invoke oblivious amplitude amplification (OAA). This requires reflections defined by Π_{win} and $|r_h\rangle$, the ancilla reference used at the beginning of each segment. Define the two reflections

$$R_{\text{win}} := I - 2\Pi_{\text{win}}, \quad R_r := 2(|r_h\rangle \langle r_h| \otimes I) - I. \quad (37)$$

Both are implementable with ancilla-only controls. The OAA applies iterations

$$Q_k := -R_r \mathcal{U}_k^\dagger R_{\text{win}} \mathcal{U}_k. \quad (38)$$

In the two-dimensional invariant subspace spanned by $|G_k\rangle$ and $|B_k\rangle$, Q_k acts as a rotation that moves $|r_{\text{win}}\rangle$ to $|r_h\rangle$.

Operationally, in the subspace $\text{span}(|G_k\rangle, |B_k\rangle)$, (Q_k) performs a Grover rotation that amplifies the Π_{win} (‘good’) component of $\mathcal{U}_k |\Psi_k\rangle$; an additional ancilla-only unitary then restores the amplified window state $|r_{\text{win}}\rangle / |r_{\text{win}}|$ to $|r_h\rangle$.

OAA requires $\Theta\left(\frac{1}{\sqrt{p_k}}\right)$ rounds to increase $\sqrt{p_k}$ to 1. In each segment, the raw success probability factors as $p_k \approx P_{\text{win}}(j_*) \|\mathbf{x}(t_{k+1})\|^2 / \|\mathbf{x}(t_k)\|^2$ (up to the exponentially small light-cone leakage into win), so the OAA iteration count scales like $1/\sqrt{p_k}$. By choosing j_* (equivalently, the window) so that $P_{\text{win}}(j_*) \geq \Delta = \Omega(1)$, we ensure that the window overlap contributes only a constant amplification overhead. Thus, with a renormalization after each segment, the OAA overhead per segment scales like

$$R_k = \mathcal{O}\left(\max\left\{1, \frac{\|\mathbf{x}(t_k)\|}{\|\mathbf{x}(t_{k+1})\|}\right\}\right). \quad (39)$$

For monotone dissipative dynamics ($\|\mathbf{x}(t)\|$ nonincreasing) the cumulative amplification overhead is

$$\prod_k \|\mathbf{x}(t_k)\| / \|\mathbf{x}(t_{k+1})\| = \|\mathbf{x}(0)\| / \|\mathbf{x}(T)\|.$$

Another interesting scenario is when the solution goes through transient growth. If $\|\mathbf{x}(t)\|$ is *not* monotone and exhibits transient amplification before decaying, then (39) shows that OAA is only costly on segments where the norm *decreases*. One may therefore omit amplification on growth segments (where p_k is larger), and apply OAA only after the trajectory passes a local maximum. For example, when $\|\mathbf{x}(t)\|$ experiences a transient growth followed by a stabilized path with a ‘‘hump’’ profile, the total amplification overhead is controlled by the peak-to-final ratio,

$$\prod_k \max\left\{1, \frac{\|\mathbf{x}(t_k)\|}{\|\mathbf{x}(t_{k+1})\|}\right\} = \frac{\sup_{t \in [0, T]} \|\mathbf{x}(t)\|}{\|\mathbf{x}(T)\|}. \quad (40)$$

Define the cumulative amplification factor

$$\Gamma := \prod_{k=0}^{N-1} \max\left\{1, \frac{\|\mathbf{x}(t_k)\|}{\|\mathbf{x}(t_{k+1})\|}\right\}. \quad (41)$$

Theorem 4 (Query complexity via segmentation + OAA). *Assume block encodings of $H(t)$ and $K(t)$, choose $\delta \geq \delta_0 > 0$ so that $\|F_h\| = \Theta(1)$. Let τ satisfy (32), and let $N = \lceil T/\tau \rceil$. Choose (M, j_*) so that $P_{\text{win}}(j_*) \geq \Delta = \Omega(1)$ and the light-cone leakage per segment and Hamiltonian simulation error is $\epsilon_{\text{seg}} \leq \Theta(\epsilon/N)$.*

(i) Non-autonomous dynamics. *There is a segmented algorithm based on Dyson-series time-dependent simulation of \mathcal{U}_k and OAA restoration such that the total number of block-encoding queries is*

$$Q^{(\text{td})} = \mathcal{O}\left(\left(H_{\max}T + K_{\max}T\right) \frac{\log(\Lambda_\tau K_{\max}T/\epsilon)}{\log \log(\Lambda_\tau K_{\max}T/\epsilon)} \Gamma\right), \quad \Lambda_\tau := H_{\max}\tau + O(1). \quad (42)$$

where Γ is defined in (41). In particular, if $K(t) \leq 0$ for all t then $\Gamma = \|\mathbf{x}(0)\| / \|\mathbf{x}(T)\|$.

(ii) Autonomous dynamics. *If $H(t) \equiv H$ and $K(t) \equiv K$, then using qubitization/QSVT per segment yields*

$$Q^{(\text{ti})} = \mathcal{O}\left(\left(\|H\| + \|K\|\right)T + \|K\|T \log(\|K\|T/\epsilon)\right) \Gamma. \quad (43)$$

Proof sketch. Fix $\epsilon_{\text{seg}} = \Theta(\epsilon/N) = \Theta(\epsilon/(K_{\max}T))$ and apply Hamiltonian simulation algorithms to each segment. \square

Complexity perspective. From a resource-scaling viewpoint, the segmented tight-binding dilation inherits the near-optimal precision dependence of interaction-picture simulation: the overhead in ϵ enters only through the standard $\log(\cdot) / \log \log(\cdot)$ factor from truncated Dyson-series techniques. In contrast, a direct LCHS-based LCU embeddings express the non-unitary propagator as a spectral integral over Hamiltonian evolutions, and after smoothing and quadrature, this typically introduces an *additional* polylogarithmic overhead in the target accuracy [1]. In the autonomous setting, qubitization/QSVT applied segment-wise yields an *additive* logarithmic dependence on $1/\epsilon$ governed by the dissipative scale (the $\log(1/\epsilon)$ term is weighted by $\|K\|T$, not by $\|H\|T$). Therefore, for weakly dissipative and autonomous problems, our complexity is slightly better. Finally, in the unitary limit $K \rightarrow 0$ the dilation becomes unnecessary and we recover the optimal Hamiltonian-simulation scaling for e^{-iHT} (up to the usual additive $\log(1/\epsilon)$ term).

E. Numerical Illustration: 2-D Maxwell Viscoelasticity model

Here we present a numerical test to demonstrate the performance of the dilation scheme in the previous section. We consider wave propagation in a 2D solid with viscoelastic behavior. The model involves a stress-strain pair (σ, ϵ) , augmented by an internal variable γ . The variables obey Maxwell type constitutive relations:

$$\sigma = K_1(\epsilon - \gamma), \quad \eta\dot{\gamma} = \sigma - K_2\gamma.$$

Here, K_1 is the series elastic modulus, K_2 is the parallel elastic modulus, and η is the viscosity [25]. To express the PDEs in the form of (1) with the decomposition (2), we define a new state vector $\mathbf{u} = (u_1, \mathbf{u}_2, u_3)^T$ where:

$$u_1 = \sqrt{K_1}(\epsilon - \gamma), \quad \mathbf{u}_2 = \sqrt{\rho^{-1}}\mathbf{p}, \quad u_3 = \sqrt{K_2}\gamma,$$

and we have denoted the momentum as $\mathbf{p} = (p_x, p_y)^T$.

The coupled PDEs for the transformed state vector \mathbf{u} can be expressed in the first-order form

$$\frac{\partial}{\partial t} \begin{pmatrix} u_1 \\ \mathbf{u}_2 \\ u_3 \end{pmatrix} = \left(\underbrace{\begin{pmatrix} 0 & \frac{\sqrt{K_1}}{\sqrt{\rho}} \nabla \cdot & 0 \\ \frac{\sqrt{K_1}}{\sqrt{\rho}} \nabla & 0 & 0 \\ 0 & 0 & 0 \end{pmatrix}}_{-iH} + \underbrace{\begin{pmatrix} -K_1/\eta & 0 & \sqrt{K_1 K_2}/\eta \\ 0 & 0 & 0 \\ \sqrt{K_1 K_2}/\eta & 0 & -K_2/\eta \end{pmatrix}}_K \right) \begin{pmatrix} u_1 \\ \mathbf{u}_2 \\ u_3 \end{pmatrix} \quad (44)$$

To maintain the structure of these operators, we apply a direct finite-difference scheme to approximate the gradient and divergence on a 2D grid in the domain $[0, 2] \times [0, 2]$ with 64 grid points in each direction. The total number of unknowns is thus $N = 16384$.

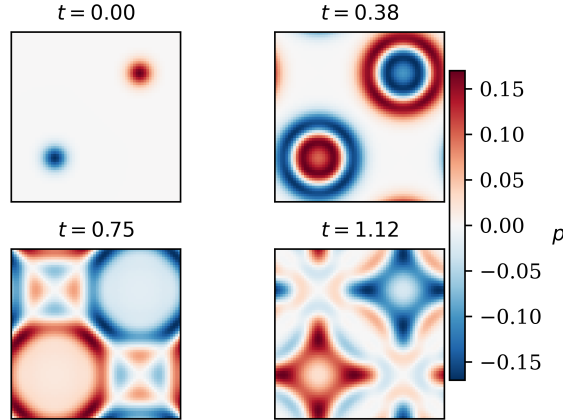


FIG. 3. Snapshot of the pressure field $p = -K(\epsilon - \gamma)$ in a 2×2 periodic domain.

In the numerical experiments, the following parameters are chosen

$$K_1 = K_2 = 1, \quad \rho = 1, \quad \eta = 3.4.$$

For the initial configuration, we prepare the volumetric strain as the difference of two Gaussian bumps

$$\epsilon = (x, y, 0) = e^{-[(x-0.5)^2 + (y-0.5)^2]/(2\sigma_0^2)} - e^{-[(x-1.5)^2 + (y-1.5)^2]/(2\sigma_0^2)}, \quad \sigma_0 = 0.05,$$

while $\mathbf{p} = \gamma = 0$. Each hump emits a cylindrical acoustic wave, and because of the periodic boundary condition, wraps around the domain. Fig. 3 shows four snapshots at various time steps, illustrating outward propagation, wrap-around interference, and attenuation.

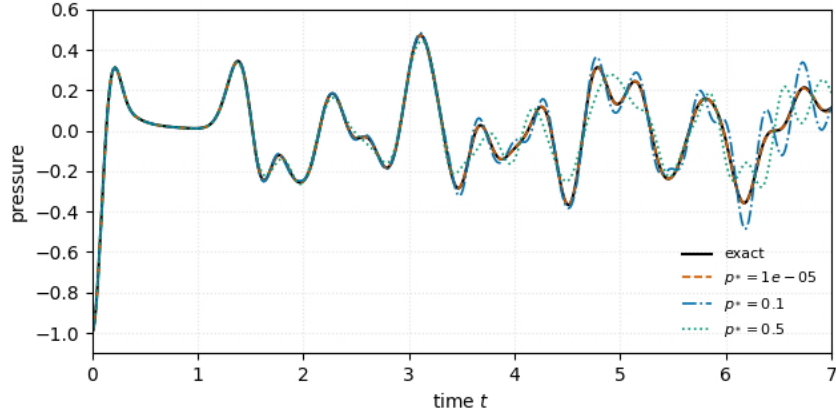


FIG. 4. Pressure time series at $(x, y) = (1/4, 1/4)$ for the Maxwell viscoelastic wave. Colored curves show the dilated dynamics for varying readout points p_* . Smaller p_* tracks the reference for longer times, while larger p_* leads to earlier deviations, illustrating the boundary light-cone effect.

To benchmark the tight-binding dilation, we couple this system to an ancilla using F_h on a geometric grid (25). For fixed M and δ , we vary the post-selection point p_* in the ancilla. Figure 4 compares the pressure signal $p(t)$ at $(x, y) = (1/4, 1/4)$ for several choices of p_* . For small p_* the dilated trajectory is visually indistinguishable from the reference solution over the entire time interval, while for larger p_* deviations appear earlier. In the appendix we show that this behavior confirms the causal structure of the lattice embedding: where the boundary-induced error is exponentially suppressed in $\frac{2eK_{\max}T}{(M-j_*)\sinh(\delta/2)}$ with j_* being the readout site. The simulations are performed classically with a Runge-Kutta time integrator and a small time step so that the time discretization error is negligible. Because the dilated Hamiltonian requires only nearest-neighbor interactions in the ancilla, we expect these dynamics to be implementable on near-term digital quantum devices without complex connectivity overhead. The code used to generate these results is available at Ref. [28].

All these numerical simulations are performed on classical computers using fourth-order Runge-Kutta methods with a small step size to remove the time integrator error from the dilation error. Due to the sparse structure of the dilate Hamiltonian, we anticipate that these simulations can also be performed on near-term quantum devices. The code is available at [28].

IV. DILATION WITH A BARGMANN–FOCK ANCILLA

Jin and Liu [19] proposed an operator F_θ that uses the momentum quadrature \hat{p} to construct the dilated Hamiltonian for analog quantum platforms. Here we present a dilation scheme, where the operator F and state $|r\rangle$ are naturally suited for realization on photonic quantum computing platforms.

Let $\mathcal{H}_A = \mathcal{B}$ be the Bargmann–Fock space of entire functions [13], with inner product $\langle f, g \rangle = \int_{\mathbb{C}} f(z)^* g(z) e^{-|z|^2} d^2z$. Here $\hat{a} = \partial_z$ and $\hat{a}^\dagger = z$. For any $\theta > 0$ define

$$F_\theta = \theta(z - \partial_z), \quad |r_\theta\rangle = \exp\left(\frac{1}{2}z^2 - \frac{z}{\theta}\right), \quad (l|f = f(0). \quad (45)$$

Because $(z - \partial_z)e^{\frac{1}{2}z^2 - \mu z} = \mu e^{\frac{1}{2}z^2 - \mu z}$, choosing $\mu = 1/\theta$ yields $F_\theta|r_\theta\rangle = |r_\theta\rangle$, so the moment identities (6) hold exactly and the dilation is exact for every θ . As a test case we take the four-site \mathcal{PT} -SSH dimer, similar to [43],

$$H = \begin{pmatrix} \delta & J_1 & 0 & 0 \\ J_1 & 0 & J_2 & 0 \\ 0 & J_2 & \delta & J_1 \\ 0 & 0 & J_1 & 0 \end{pmatrix}, \quad K = \gamma \text{diag}(1, 0, 1, 0), \quad (46)$$

with $(J_1, J_2, \delta, \gamma) = (1.0, 0.6, 0.3, -1/16)$ and $T = 0.5$. As a result, the dilated Hamiltonian \tilde{H} acts on five qumodes (one ancilla).

Toward a continuous-variable (CV) realization, we simulate \tilde{H} on a single CV mode (the ancilla) plus four qumodes for the SSH chain using the STRAWBERRY FIELDS package [23] for photonic quantum computing platforms. We initialize the solution state in the vacuum, $\mathbf{x}_0 = |0\rangle$, then prepare $|e_r\rangle$ with a squeezing gate, $\text{Sgate!}(r = \frac{1}{2} \ln 2)$, followed by a displacement gate, $\text{Dgate!}(\alpha = -1/(\sqrt{2}, \theta))$. Throughout, we set $\theta = 0.5$ and truncate the Fock basis at five photons. We then evolve the dilated Hamiltonian with a symmetric second-order Trotter method with step size $\Delta t = 0.025$. In each time step, we apply an on-site rotations $R(\pm \delta \Delta t)$, beam-splitters for the off diagonals J_1 and J_2 and the loss coupling, implemented by sandwiching $V(\pi/2) \text{CX}(-\gamma \Delta t) V(-\pi/2)$, where $V(\phi) = e^{i\phi x^3}$. As an observable, we measure the ancilla with `MeasureFock` and compute $\rho_{\text{edge}}(t) = |x_1(t)|^2$.

As shown in Fig. 5, the CV data (markers) and exact solution (solid line) shows reasonable agreement, confirming the feasibility of the Bargmann–Fock dilation method.

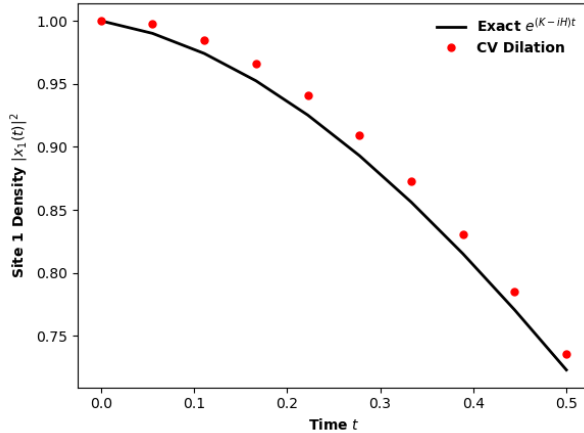


FIG. 5. Edge-density dynamics for the \mathcal{PT} -SSH dimer: simulation using CV dilation (dots) vs. exact results using matrix exponential (solid).

V. FURTHER DISCUSSIONS

A. Implementation by LCU

Our dilation admits a linear-combination-of-unitaries (LCU) form that is closely related to the linear combination of Hamiltonian simulation (LCHS) technique [1, 2], but arises from a different spectral transform (Mellin rather than Fourier). Assume the interior generator F admits the spectral resolution

$$F = -i \int_{\mathbb{R}} \omega |\psi_{\omega}\rangle \langle \psi_{\omega}| d\mu(\omega), \quad (47)$$

so that $iF = \int \omega |\psi_{\omega}\rangle \langle \psi_{\omega}| d\mu$. Then the dilated Hamiltonian factorises as

$$I_A \otimes H(t) + iF \otimes K(t) = \int_{\mathbb{R}} |\psi_{\omega}\rangle \langle \psi_{\omega}| \otimes (H(t) + \omega K(t)) d\mu(\omega).$$

Consequently, for any left-right test vectors $(l|, |r)$ and initial state $|\mathbf{x}_0\rangle$,

$$\begin{aligned} & ((l| \otimes I) \mathcal{T} \exp \left(-i \int_0^T [I_A \otimes H(s) + iF \otimes K(s)] ds \right) (|r) \otimes |\mathbf{x}_0\rangle) \\ &= \int_{\mathbb{R}} [(l|\psi_{\omega}) [(\langle \psi_{\omega}| |r)] \mathcal{T} e^{-i \int_0^T (H(s) + \omega K(s)) ds} |\mathbf{x}_0\rangle d\mu(\omega). \end{aligned} \quad (48)$$

Equation (48) is an LCHS-type integral representation: after quadrature in ω , one obtains a concrete LCU over propagators of the form $\mathcal{T}e^{-i\int(H+\omega K)}$.

For the differential operator F , the Mellin-wave basis [9]

$$\psi_\omega(p) = p^{-1/2-i\omega}, \quad \omega \in \mathbb{R},$$

satisfies $F\psi_\omega = -i\omega\psi_\omega$, and $d\mu(\omega) = d\omega/(2\pi)$, so (47) is precisely the Mellin transform of F .

A fully discrete LCU form also appears after the discretization on the SBP stencil. Since the grid length $M = \Omega(\log(1/\epsilon))$ is modest, we can *classically* diagonalise the interior matrix $F_h \in \mathbb{C}^{(M+1) \times (M+1)}$:

$$F_h = -i \sum_{j=0}^M \omega_j |\phi_j\rangle \langle \phi_j|, \quad \omega_j \in \mathbb{R}, \quad \{|\phi_j\rangle\}_{j=0}^M \text{ orthonormal.} \quad (49)$$

Then

$$I_A \otimes H(t) + iF_h \otimes K(t) = \sum_{j=0}^M |\phi_j\rangle \langle \phi_j| \otimes (H(t) + \omega_j K(t)),$$

and the time-ordered propagator decomposes as

$$U(t) = \sum_{j=0}^M |\phi_j\rangle \langle \phi_j| \otimes \mathcal{T}e^{-i \int_0^t (H(s) + \omega_j K(s)) ds}.$$

Hence, for the dilation-consistent pair

$$|r_h\rangle = |r_h\rangle = \frac{1}{\sqrt{S}} \sum_{j=0}^M \sqrt{w_j} |j\rangle, \quad \langle l_h| = \sqrt{\frac{S}{S_W}} \langle l_h|, \quad \langle l_h| = \frac{1}{\sqrt{S_W}} \sum_{j=0}^{j_*} \sqrt{w_j} \langle j|, \quad (50)$$

with normalizing constants $S_W = \sum_{j=0}^{j_*} w_j$, $S = \sum_{j=0}^M w_j$ we obtain the explicit LCU expansion

$$|\mathbf{x}(t)\rangle = \sum_{j=0}^M \underbrace{\langle l_h| \phi_j \rangle \langle \phi_j | r_h \rangle}_{=:c_j} \mathcal{T}e^{-i \int_0^t (H(s) + \omega_j K(s)) ds} |\mathbf{x}_0\rangle = \sum_j c_j U_j(t) |\mathbf{x}_0\rangle. \quad (51)$$

By Cauchy-Schwarz with the orthonormal basis $\{|\phi_j\rangle\}$,

$$\|\mathbf{c}\|_1 \leq \|l_h\| \|r_h\| = \frac{\sqrt{S}}{\sqrt{S_W}} = \frac{1}{\sqrt{P_{\text{win}}(j_*)}}, \quad P_{\text{win}}(j_*) := \frac{S_W}{S}.$$

Thus a direct (single-shot) LCU implementation has success amplitude scaling like $\sqrt{P_{\text{win}}}$; if the window weight P_{win} is tiny, the LCU ℓ_1 -weight $\|\mathbf{c}\|_1$ is large. A standard remedy is time segmentation: split $[0, T]$ into L segments of length $\tau = \Theta(1/K_{\text{max}})$, apply LCU on each segment (so that ℓ_1 -weights per segment are $\mathcal{O}(1)$), use robust oblivious amplitude amplification (OAA) per segment, and coherently *restore* the ancilla back to $|r_h\rangle$ at the end of each segment. In this way the per-segment LCU ℓ_1 -weight L_{seg} can be kept ≤ 2 (cf. [34, Sec. 3]), yielding an overall near-optimal scaling when combined with the Dyson-series interaction-picture framework in the previous subsection.

B. ODEs with transient or persistent growth

Most earlier quantum algorithms target *dissipative* ODEs where $K \prec 0$, so solutions are contractive (e.g., [2, 21]). Even for an autonomous *stable* system $\mathbf{x}'(t) = A\mathbf{x}(t)$ whose spectrum lies in the closed left half-plane (and purely imaginary eigenvalues are simple), non-normality can cause substantial *transient* growth when K is not negative definite.

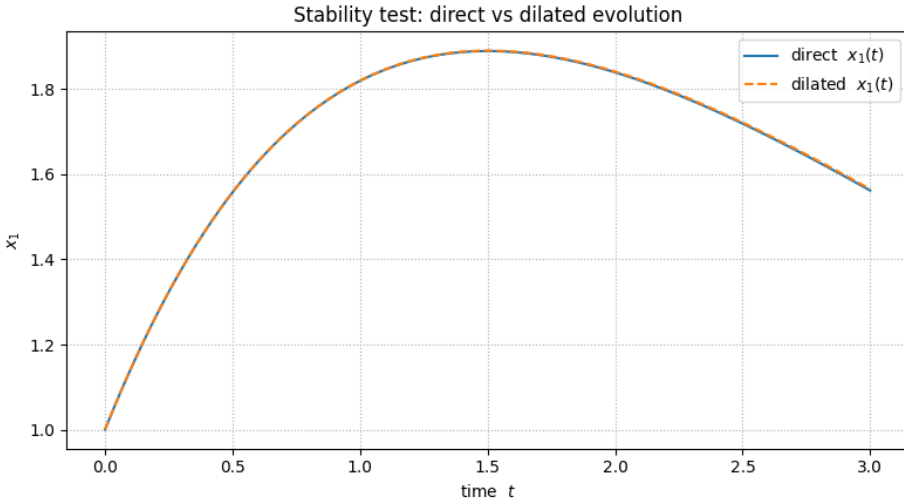


FIG. 6. Exact and dilated solutions of (52).

As a representative example, consider

$$A = \begin{bmatrix} -\frac{1}{2} & 1 \\ 0 & -\frac{1}{2} \end{bmatrix}, \quad \mathbf{x}_0 = \begin{bmatrix} 1 \\ 1 \end{bmatrix}. \quad (52)$$

The exact solution exhibits transient growth with $\|\mathbf{x}(t)\| \sim te^{-t/2}$ before decaying. We discretize the dilation using the second-order diagonal-norm SBP split form on a *geometric mesh* $p_j = \exp[-(1 - j/M)]$ with $M = 10$ points ($\delta = 1$, i.e. $\Lambda = M$). We set $\theta = 2$ ($\beta = 0$), prepare the ancilla in $|r_h\rangle \propto W^{1/2}\mathbf{1}$, and post-select at $j_* = 8$ so that $\langle l_h|r_h\rangle = 1$. Both the physical ODE and the dilated system are integrated in time by a fourth-order Runge–Kutta scheme up to $t_{\text{final}} = 3$ using $n_{\text{steps}} = 400$ (step size 7.5×10^{-3}), making the time-integration error negligible compared to the spatial/discretization effects. The ancilla-projected trajectory $x_1(t)$ from the dilated evolution matches the exact solution. This provides direct numerical evidence (complementing our main theorems) that the dilation framework also applies to ODEs with transient instability.

The dilation also applies to *unstable* ODEs with persistent growth. As a simple test, take

$$A = \begin{bmatrix} \frac{1}{2} & 1 \\ 0 & \frac{1}{2} \end{bmatrix}, \quad \mathbf{x}_0 = \begin{bmatrix} 1 \\ 1 \end{bmatrix}. \quad (53)$$

Figure 7 shows excellent agreement between the exact and dilated solutions, with the latter obtained with a similar dilation scheme as above.

VI. SUMMARY AND OUTLOOK

This paper presented a general dilation scheme that encodes the dynamics associated with an ODE or PDE into a unitary dynamics. We propose to wrap such dilation schemes through three elements, a skew Hermitian operator F , an encoding element $|r\rangle$, and an evaluation functional $\langle l|$. The seven concrete families detailed in the main text, together with flexible parameter θ and unitary transformation among the triple, illustrate the breadth of this new framework, which allows the dilation to be co-designed with the target hardware (gate-based, continuous-variable, analogue) and with the structure of a given application.

Nonlinear problems are generally difficult for quantum computing algorithms. One approach that has been extensively studied is the Carleman embedding method [7, 24, 30, 31, 42], which can be viewed as a dilation as well, where $|r\rangle$ corresponds to monomials, forming a nonlinear transformation, and $\langle l|$ can be

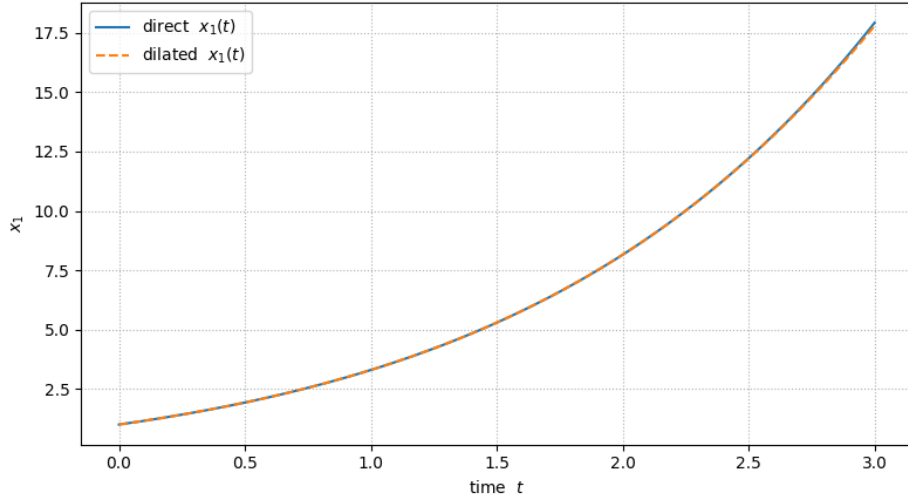


FIG. 7. Exact and dilated solutions of (53).

interpreted as the evaluation of the first monomial. It is possible that the current framework can produce other dilation schemes for nonlinear problems, and it is an interesting future direction.

Acknowledgement. This research is supported by the NSF Grant DMS-2411120.

[1] D. An, A. M. Childs, and L. Lin. Quantum algorithm for linear non-unitary dynamics with near-optimal dependence on all parameters, 2023. arXiv:2312.03916.

[2] D. An, J.-P. Liu, and L. Lin. Linear combination of Hamiltonian simulation for nonunitary dynamics with optimal state preparation cost. *Physical Review Letters*, 131(15):150603, 2023. arXiv:2303.01029.

[3] D. W. Berry. High-order quantum algorithm for solving linear differential equations. *Journal of Physics A: Mathematical and Theoretical*, 47(10):105301, 2014. arXiv:1010.2745.

[4] D. W. Berry, A. M. Childs, A. Ostrander, and G. Wang. Quantum algorithm for linear differential equations with exponentially improved dependence on precision. *Communications in Mathematical Physics*, 356(3):1057–1081, 2017. arXiv:1701.03684.

[5] D. W. Berry and P. C. Costa. Quantum algorithm for time-dependent differential equations using Dyson series. *Quantum*, 8:1369, 2024. arXiv:2212.03544.

[6] S. S. Bharadwaj and K. R. Sreenivasan. Compact quantum algorithms for time-dependent differential equations. *Physical Review Research*, 7(2):023262, 2025.

[7] N. Brüstle and N. Wiebe. Quantum and classical algorithms for nonlinear unitary dynamics. *arXiv preprint arXiv:2407.07685*, 2024.

[8] A. M. Childs and J.-P. Liu. Quantum spectral methods for differential equations. *Communications in Mathematical Physics*, 375(2):1427–1457, 2020.

[9] L. Debnath and D. Bhatta. *Integral Transforms and Their Applications*. Chapman & Hall/CRC, Boca Raton, 3rd edition, 2015. Chapters 10–11 give a self-contained treatment of the Mellin transform, including inversion, convolution, and applications to differential equations.

[10] D. Dong, Y. Li, and J. Xue. A quantum algorithm for linear autonomous differential equations via padé approximation. *Quantum*, 9:1770, 2025.

[11] D. Fang, L. Lin, and Y. Tong. Time-marching based quantum solvers for time-dependent linear differential equations. *Quantum*, 7:955, 2023. arXiv:2208.06941.

[12] A. Gilyén, Y. Su, G. H. Low, and N. Wiebe. Quantum singular value transformation and beyond: exponential improvements for quantum matrix arithmetics. In *Proceedings of the 51st annual ACM SIGACT symposium on theory of computing*, pages 193–204, 2019.

[13] B. C. Hall. *Quantum theory for mathematicians*. Springer, 2013.

[14] J. Hu, S. Jin, N. Liu, and L. Zhang. Quantum circuits for partial differential equations via schrödingerisation. *Quantum*, 8:1563, 2024.

- [15] J. Hu, S. Jin, N. Liu, and L. Zhang. Dilation theorem via schrödingerization, with applications to the quantum simulation of differential equations. *Studies in Applied Mathematics*, 154(4):e70047, 2025.
- [16] X. Huang and D. An. Fourier transform-based linear combination of hamiltonian simulation. *arXiv preprint arXiv:2508.19596*, 2025.
- [17] S. Jin, X. Li, N. Liu, and Y. Yu. Quantum simulation for partial differential equations with physical boundary or interface conditions. *Journal of Computational Physics*, 498:112707, 2024.
- [18] S. Jin, X. Li, N. Liu, and Y. Yu. Quantum simulation for quantum dynamics with artificial boundary conditions. *SIAM Journal on Scientific Computing*, 46(4):B403–B421, 2024.
- [19] S. Jin and N. Liu. Analog quantum simulation of parabolic partial differential equations using jaynes-cummings-like models. *arXiv preprint arXiv:2407.01913*, 2024.
- [20] S. Jin, N. Liu, C. Ma, and Y. Yu. On the schr\"{o}dingerization method for linear non-unitary dynamics with optimal dependence on matrix queries. *arXiv preprint arXiv:2505.00370*, 2025.
- [21] S. Jin, N. Liu, and Y. Yu. Quantum simulation of partial differential equations: Applications and detailed analysis. *Physical Review A*, 108(3):032603, 2023.
- [22] S. Jin, N. Liu, and Y. Yu. Quantum simulation of partial differential equations via Schrödingerization. *Phys. Rev. Lett.*, 133:230602, Dec 2024.
- [23] N. Killoran, J. Izaac, N. Quesada, V. Bergholm, M. Amy, and C. Weedbrook. Strawberry fields: A software platform for photonic quantum computing. *Quantum*, 3:129, 2019.
- [24] H. Krovi. Improved quantum algorithms for linear and nonlinear differential equations. *Quantum*, 7:913, 2023.
- [25] R. S. Lakes. *Viscoelastic Materials*. Cambridge University Press, Cambridge, 2009.
- [26] R. J. LeVeque and R. J. Leveque. *Numerical methods for conservation laws*, volume 132. Springer, 1992.
- [27] H. Li, H. Ni, and L. Ying. On efficient quantum block encoding of pseudo-differential operators. *Quantum*, 7:1031, 2023.
- [28] X. Li. Quantum dilation algorithms for linear odes. <https://github.com/xxl12/quantum-dilation-algorithms>, 2025. Accessed: 2025-07-12.
- [29] E. H. Lieb and D. W. Robinson. The finite group velocity of quantum spin systems. *Communications in Mathematical Physics*, 28(3):251–257, 1972.
- [30] J.-P. Liu, D. An, D. Fang, J. Wang, G. H. Low, and S. Jordan. Efficient quantum algorithm for nonlinear reaction-diffusion equations and energy estimation. *Commun. Math. Phys.*, 404(arXiv: 2205.01141):963–1020, 2023.
- [31] J.-P. Liu, H. Ø. Kolden, H. K. Krovi, N. F. Loureiro, K. Trivisa, and A. M. Childs. Efficient quantum algorithm for dissipative nonlinear differential equations. *Proceedings of the National Academy of Sciences*, 118(35):e2026805118, 2021.
- [32] G. H. Low and I. L. Chuang. Hamiltonian simulation by qubitization. *Quantum*, 3:163, 2019. arXiv:1610.06546.
- [33] G. H. Low and R. D. Somma. Optimal quantum simulation of linear non-unitary dynamics. *arXiv preprint arXiv:2508.19238*, 2025.
- [34] G. H. Low and N. Wiebe. Hamiltonian simulation in the interaction picture. *arXiv preprint arXiv:1805.00675*, 2018.
- [35] R. Lu, H.-E. Li, Z. Liu, and J.-P. Liu. Infinite-dimensional extension of the linear combination of hamiltonian simulation: Theorems and applications. *arXiv preprint arXiv:2502.19688*, 2025.
- [36] K. Mattsson and J. Nordström. Summation by parts operators for finite difference approximations of second derivatives with variable coefficients. *Journal of Computational Physics*, 199(2):503–540, 2004.
- [37] B. S. Nagy, C. Foias, H. Bercovici, and L. Kérchy. *Harmonic analysis of operators on Hilbert space*. Springer Science & Business Media, 2010.
- [38] Q. T. Nguyen, B. T. Kiani, and S. Lloyd. Block-encoding dense and full-rank kernels using hierarchical matrices: applications in quantum numerical linear algebra. *Quantum*, 6:876, 2022.
- [39] M. Poernic, P. D. Johnson, A. Katabarwa, and N. Wiebe. Constant-factor improvements in quantum algorithms for linear differential equations. *arXiv preprint arXiv:2506.20760*, 2025.
- [40] B. Strand. Summation by parts for finite difference approximations for $\partial/\partial x$. *Journal of Computational Physics*, 110(1):47–67, 1994.
- [41] H.-C. Wu and X. Li. Structure-preserving quantum algorithms for linear and nonlinear hamiltonian systems. *arXiv preprint arXiv:2411.03599*, 2024.
- [42] H.-C. Wu, J. Wang, and X. Li. Quantum algorithms for nonlinear dynamics: Revisiting carleman linearization with no dissipative conditions. *SIAM Journal on Scientific Computing*, 47(2):A943–A970, 2025.
- [43] S. Yao and Z. Wang. Edge states and topological invariants of non-hermitian systems. *Physical review letters*, 121(8):086803, 2018.

Appendix A: Lightcone property of the finite difference operator

This section is dedicated to the error bound Theorem 5, which we will prove by separating the approximation error of the differential operator and the boundary error.

The dilation method involves the following partial differential equation,

$$u_t = -\theta\kappa(t)(pu_p + \frac{1}{2}u), \quad u(t, 1) = u_R(t), \quad (\text{A1})$$

with solution $u(t, p) : [0, +\infty) \otimes [0, 1] \mapsto \mathbb{R}$. $\theta > 0$ is a numerical parameter that we will choose to optimize our quantum algorithms later. This is a first-order PDE, and the solution can be constructed by the method of characteristics. When $\kappa(t)$ is positive, the solution propagates to the left and $u_R(t)$ acts as the boundary condition. For convenience, we write

$$u_t = -\kappa(t)F_\theta u, \quad F_\theta = \theta F, \quad (\text{A2})$$

with the partial differential operator given by, for any differentiable function $v(p)$,

$$Fv(p) := (p\partial_p v(p) + \frac{1}{2}v(p)). \quad (\text{A3})$$

The time-dependent coefficients $-\kappa(t)$ will be generalized to a Hermitian negative definite matrix $K(t)$ later in this section.

To obtain a direct numerical method, we partition the unit interval into M subintervals, and find approximation solutions on a uniform grid with grid size denoted by h ,

$$p_i = ih, h = \frac{1}{M}, \quad 0 \leq i \leq M. \quad (\text{A4})$$

To construct an approximation to the solution of Eq. (A2), we construct a difference operator on the grid, as follows, denoting $v_i := v(p_i)$,

$$\begin{aligned} (F_h \mathbf{v})_0 &= \frac{1}{4\sqrt{2}}v_1, \\ (F_h \mathbf{v})_1 &= \frac{3}{4}v_2 - \frac{1}{4\sqrt{2}}v_0, \\ (F_h \mathbf{v})_i &= \frac{p_{i+1} + p_i}{4h}v_{i+1} - \frac{p_i + p_{i-1}}{4h}v_{i-1}, \quad 2 \leq i \leq M-1, \\ (F_h \mathbf{v})_M &= -\frac{p_M + p_{M-1}}{4h}v_{M-1}. \end{aligned} \quad (\text{A5})$$

The coefficients $\frac{1}{4\sqrt{2}}$ come from the quadrature approximation in the summation by parts methods [36, 40].

The following property can be easily verified by using integration/summation by parts.

Lemma 4. *With zero boundary condition, $v(1) = 0$, both operators F in Eq. (A3) and Eq. (A5) are skew Hermitian.*

In the next few sections, we explain several approximation properties of F_h in approximating the solution of the PDE (A2).

1. Finite-Propagation Property of the Semi-Discrete Scheme

One important property of the PDE Eq. (A1) is the finite propagation speed and finite domain of influence. According to the method of characteristics, $-\theta\kappa(t)$ is regarded as the propagation speed of the solution moving to the left. For example, if $\kappa(t)$ is always bounded by $\frac{1}{4T}$, then the part of the initial condition $u(0, p)$ that lies in $p \in (\frac{3}{4}, 1)$ would have no impact on the solution $u(T, p)$ for $p \in (0, \frac{1}{2})$.

As a simple demonstration, consider the first-order linear PDE

$$u_t = -pu_p - \frac{1}{2}u, \quad 0 < p < 1, \quad t \geq 0.$$

Its behaviour is completely transparent through the *method of characteristics*. One can find the solution by following a family of trajectories $(p(t), t)$, satisfying $\frac{dp}{dt} = -p$, and along these trajectories, the solution of the above PDE is reduced to the solution of the ODEs (by chain rule)

$$\frac{du}{dt} = -\frac{1}{2}u.$$

The first equation integrates to an exponential

$$p(t) = p_0 e^{-(t-t_0)} \implies t - t_0 = \ln \frac{p_0}{p(t)}.$$

Thus every “signal” injected at some point p_0 travels *inward* with speed proportional to the current p ; it needs the finite time

$$T(p_0 \rightarrow p_*) = \ln \frac{p_0}{p_*}$$

to reach a location $p_* < p_0$. Meanwhile, the second ODE for u gives exponential damping along the same curve,

$$u(p(t), t) = u(p_0, t_0) \exp\left[-\frac{1}{2}(t - t_0)\right].$$

Take $p_0 = 1$ (the boundary) and impose $u(1, t) = 1$. These equations describe the disturbance at the boundary that first hits the interior point p_* exactly at time

$$T_{\text{arrive}} = \ln \frac{1}{p_*}, \quad (\text{A6})$$

no sooner: One remarkable consequence is that such disturbance takes infinite time to arrive at $p = 0$.

We now establish a finite-propagation-speed estimate for the discrete scheme. The bound shows that the influence of the right-hand boundary condition at $p = 1$ decays exponentially as one moves into the interior of the grid, playing the same role for our numerical solution that the Lieb–Robinson bound [29] plays in quantum lattice systems.

Lemma 5 (Finite propagation speed bound). *Fix $\theta > 0$ and assume the modulation $0 \leq \kappa(t) \leq K_{\max}$ on the whole interval $[0, T]$. Let $p_* \in (0, 1)$ be an interior abscissa and suppose the travel-time condition*

$$e\theta K_{\max} T < 1 - p_* \quad (\text{A7})$$

holds. Start from the canonical right-boundary vector $\mathbf{u}^R = (0, \dots, 0, 1)^T = |M\rangle$. Then for every $t \in [0, T]$ and every grid index i with $p_i \leq p_$ the propagated amplitude satisfies*

$$|\langle i | e^{-\int_0^t \theta \kappa(s) ds F_h} | \mathbf{u}^R \rangle| \leq \frac{\left(\frac{e\theta K_{\max} T}{1-p_*}\right)^m}{1 - \frac{e\theta K_{\max} T}{1-p_*}}, \quad m = M - i.$$

Proof. Write $F_h = B_+ - B_-$ where $(B_+)_k, k+1 = (p_{k+1} + p_k)/(4h)$ and $(B_-)_{k,k-1} = (p_k + p_{k-1})/(4h)$. Each product of k factors moves information at most k nodes, hence $\langle i | F_h^k | M \rangle = 0$ whenever $k < m$.

Because $(p_r + p_s) \leq 2$ and every row has two non-zero entries,

$$\|F_h\|_\infty \leq \frac{1}{h}, \quad \implies \quad \|F_h^k\|_\infty \leq h^{-k}.$$

Combining these observations, we have

$$|\langle i | e^{-\int_0^t \theta \kappa(s) ds F_h} | M \rangle| \leq \sum_{k=m}^{\infty} \frac{(\theta K_{\max} t/h)^k}{k!}.$$

Using Stirling's bound $k! \geq (k/e)^k$ we simplify each term to $\frac{(\theta K_{\max} t/h)^k}{k!} \leq \left(\frac{e\theta K_{\max} t}{hk}\right)^k$. For $k = m$ and $hm \geq 1 - p_*$ (because $p_i \leq p_*$) this ratio is bounded by

$$\frac{e\theta K_{\max} t}{hm} \leq \frac{e\theta K_{\max} t}{1 - p_*} < 1,$$

where the last inequality is the travel-time hypothesis (A7). Summing the geometric tail yields the stated exponential bound. \square

This finite propagation estimate can be directly generalized to bound the error due to the homogeneous boundary condition that helps to ensure the Hermitian property of the dilated Hamiltonian. To the error from the interior, let us first consider the following dynamics:

$$\frac{d}{dt} \chi(t) = (-iI_A \otimes H(t) + \theta F_h \otimes K(t))\chi(t) + \alpha |M\rangle \otimes K(t)\mathbf{x}(t), \quad \chi(0) = 0. \quad (\text{A8})$$

The first term on the right hand side in Eq. (A8) is the dilated Hamiltonian, while the second term, which only concentrates at the boundary, comes from the effect of dropping the boundary condition with some positive constant α . In particular, it carries the solution of the ODE: $\mathbf{x}(t)$. How Eq. (A8) emerges from the global error analysis will be elaborated in the next section.

Lemma 6 (Finite propagation speed bound for the dilated system). *Fix $\theta > 0$ and $K_{\max} := \max_{t \in [0, T]} \|K(t)\|$. Let $p_* \in (0, 1)$ be an interior abscissa and assume the travel-time condition (A7) from Lemma 5,*

$$e\theta K_{\max} T < 1 - p_*.$$

Fix an interior evaluation point $p_* = p_i \in (0, 1)$ and set $m := M - i = (1 - p_*)/h$. Consider χ governed by

$$\frac{d}{dt} \chi(t) = (-iI_A \otimes H(t) + \theta F_h \otimes K(t))\chi(t) + \alpha |M\rangle \otimes K(t)\mathbf{x}(t), \quad \chi(0) = 0. \quad (\text{A9})$$

Then, for every $T \in [0, \infty)$,

$$\|(\langle i | \otimes I)\chi(T)\| \leq \alpha K_{\max} X(T) \|\mathbf{x}(0)\| T \cdot \frac{\left(\frac{e\theta K_{\max} T}{1 - p_*}\right)^m}{1 - \frac{e\theta K_{\max} T}{1 - p_*}}, \quad (\text{A10})$$

where $X(T) := \max_{t \in [0, T]} \|\mathbf{x}(t)\|/\|\mathbf{x}(0)\|$. Consequently, if $\varrho := \frac{e\theta K_{\max} T}{1 - p_*} < 1$, then for any $\epsilon > 0$ it suffices to choose

$$m \geq \left\lceil \frac{\ln(\alpha K_{\max} X(T) \|\mathbf{x}(0)\| T / (\epsilon(1 - \varrho)))}{\ln(1/\varrho)} \right\rceil$$

to guarantee $\|(\langle i | \otimes I)\chi(T)\| \leq \epsilon$.

Proof. We first eliminate the $I_A \otimes H$ term in Eq. (A9) by working in the interaction picture. Let $U_H(t)$ solve $U'_H(t) = -iH(t)U_H(t)$ with $U_H(0) = I$, and define the interaction-picture quantities

$$K_I(t) := U_H(t)^\dagger K(t)U_H(t), \quad \mathbf{x}_I(t) := U_H(t)^\dagger \mathbf{x}(t), \quad \chi_I(t) := (I_A \otimes U_H(t)^\dagger)\chi(t).$$

Since $U_H(t)$ is unitary, $\|K_I(t)\| = \|K(t)\|$ and $\|\mathbf{x}_I(t)\| = \|\mathbf{x}(t)\|$.

Then (A9) becomes the inhomogeneous linear ODE

$$\frac{d}{dt} \chi_I(t) = (\theta F_h \otimes K_I(t))\chi_I(t) + \alpha |M\rangle \otimes K_I(t)\mathbf{x}_I(t), \quad \chi_I(0) = 0. \quad (\text{A11})$$

Let $W(T, t)$ denote the fundamental (propagator) solution of the homogeneous part,

$$\partial_T W(T, t) = (\theta F_h \otimes K_I(T))W(T, t), \quad W(t, t) = I.$$

Variation of constants gives

$$\chi_I(T) = \alpha \int_0^T W(T, t) |M\rangle \otimes K_I(t) \mathbf{x}_I(t) dt. \quad (\text{A12})$$

Because F_h is time-independent, the Dyson (time-ordered) series for $W(T, t)$ reads

$$W(T, t) = I + \sum_{k=1}^{\infty} \theta^k \underbrace{\int_{t \leq t_1 \leq \dots \leq t_k \leq T} (F_h \otimes K_I(t_k)) \cdots (F_h \otimes K_I(t_1)) dt_1 \cdots dt_k}_{=: \mathcal{J}_k(T, t)}. \quad (\text{A13})$$

Since F_h commutes with itself,

$$\mathcal{J}_k(T, t) = F_h^k \otimes \left(\int_{t \leq t_1 \leq \dots \leq t_k \leq T} K_I(t_k) \cdots K_I(t_1) dt_1 \cdots dt_k \right) = F_h^k \otimes J_k(T, t),$$

where, with the convention $J_0(T, t) := I$,

$$J_k(T, t) := \int_{t \leq t_1 \leq \dots \leq t_k \leq T} K_I(t_k) \cdots K_I(t_1) dt_1 \cdots dt_k. \quad (\text{A14})$$

Thus,

$$W(T, t) = \sum_{k=0}^{\infty} \theta^k F_h^k \otimes J_k(T, t). \quad (\text{A15})$$

Insert (A15) into (A12):

$$\chi_I(T) = \alpha \sum_{k=0}^{\infty} \theta^k F_h^k |M\rangle \otimes \left(\int_0^T J_k(T, t) K_I(t) \mathbf{x}_I(t) dt \right).$$

Apply $(\langle i | \otimes I)$ and use the band structure of F_h :

$$\langle i | F_h^k | M \rangle = 0 \quad \text{for all } k < m, \quad m := M - i, \quad (\text{A16})$$

so only the terms with $k \geq m$ remain:

$$(\langle i | \otimes I) \chi_I(T) = \alpha \sum_{k=m}^{\infty} \theta^k \langle i | F_h^k | M \rangle \left(\int_0^T J_k(T, t) K_I(t) \mathbf{x}_I(t) dt \right). \quad (\text{A17})$$

We recall the uniform bound from Lemma 5: since each row of F_h has at most two nonzero entries of size $\leq 1/(2h)$,

$$\|F_h\| \leq \frac{1}{h} \implies \|F_h^k\| \leq h^{-k}.$$

Also, $\|K_I(t)\| \leq K_{\max}$ and $\|\mathbf{x}_I(t)\| \leq X(T)$. For the time-ordered integrals (A14),

$$\|J_k(T, t)\| \leq \int_{t \leq t_1 \leq \dots \leq t_k \leq T} \|K_I(t_k) \cdots K_I(t_1)\| dt_1 \cdots dt_k \leq \frac{(K_{\max})^k}{k!} (T - t)^k.$$

Therefore,

$$\left\| \int_0^T J_k(T, t) K_I(t) \mathbf{x}_I(t) dt \right\| \leq \int_0^T \frac{(K_{\max})^k}{k!} (T - t)^k K_{\max} X(T) dt = \frac{(K_{\max} T)^{k+1}}{(k+1)!} K_{\max} X(T).$$

Combining with $\|\langle i | F_h^k | M \rangle\| \leq \|F_h^k\|_\infty \leq h^{-k}$, (A17) yields

$$\|(\langle i | \otimes I) \chi_I(T)\| \leq \alpha K_{\max} X(T) T \sum_{k=m}^{\infty} \frac{(\theta K_{\max} T/h)^k}{(k+1)!}.$$

Use $(k+1)! \geq k!$ to get the simpler tail

$$\sum_{k=m}^{\infty} \frac{(\theta K_{\max} T/h)^k}{(k+1)!} \leq \sum_{k=m}^{\infty} \frac{(\theta K_{\max} T/h)^k}{k!}.$$

Now apply Stirling's bound $k! \geq (k/e)^k$ as in Lemma 5:

$$\frac{(\theta K_{\max} T/h)^k}{k!} \leq \left(\frac{e \theta K_{\max} T}{h k} \right)^k.$$

For $k \geq m$ and $h m \geq 1 - p_*$ (since $p_i \leq p_*$), we obtain the uniform ratio

$$\left(\frac{e \theta K_{\max} T}{h k} \right)^k \leq \left(\frac{e \theta K_{\max} T}{1 - p_*} \right)^k =: \varrho^k, \quad \varrho = \frac{e \theta K_{\max} T}{1 - p_*} < 1$$

by the travel-time hypothesis (A7). Summing the geometric tail gives

$$\sum_{k=m}^{\infty} \frac{(\theta K_{\max} T/h)^k}{k!} \leq \frac{\varrho^m}{1 - \varrho}.$$

Inserting this into the previous bound yields (A10) for $\|(\langle i | \otimes I) \chi_I(T)\|$, and since the physical and interaction pictures differ by a unitary on the second tensor factor, the same bound holds for $\|(\langle i | \otimes I) \chi(T)\|$. \square

2. Lightcone property on the geometric grid

Let $p_j = e^{-(M-j)\delta}$ with fixed $\delta > 0$, and let F_h be the split-form Euclidean-skew tridiagonal with off-diagonals

$$f_j = \frac{1}{4 \sinh(\delta/2)} \times \begin{cases} \sqrt{1 + e^{-\delta}}, & j = 0, \\ 1, & 1 \leq j \leq M-2, \\ \sqrt{1 + e^\delta}, & j = M-1. \end{cases}$$

We let the uniform interior weight be $f_{\text{int}} = \frac{1}{4 \sinh(\delta/2)}$.

Lemma 7. *Let F_h be the split-form tridiagonal matrix from the SBP discretization on the geometrically scaled grid with $\delta \geq 1$. $\forall j_* \in [M]$, let $m = M - j_*$. Then*

$$|\langle j_* | \chi(T) | M \rangle| \leq \frac{C(\delta) \varrho^m}{1 - \varrho^2}, \quad \varrho := \frac{e \theta K_{\max} T}{4m \sinh \frac{\delta}{2}} \quad (\text{A18})$$

where $C(\delta) = \max\{f_0, f_{M-1}\}$. $C(\delta) \leq \sup_{\delta \geq 1} \{f_{M-1}\} = \frac{\sqrt{1+e}}{4 \sinh(1/2)} \approx 0.926$.

Proof sketch. Write the split-form SBP chain as

$$F_h = \sum_{j=0}^{M-1} f_j (|j\rangle \langle j+1| - |j+1\rangle \langle j|) = A - A^\dagger, \quad A := \sum_{j=0}^{M-1} f_j |j\rangle \langle j+1|.$$

Thus A lowers the site index by one (a left hop) with weight f_j , while $-A^\dagger$ raises the index by one (a right hop) with weight f_j and an extra minus sign. Fix $j_* \leq M$ and set $m := M - j_*$. For every integer $k \geq m$,

$\langle j_* | F_h^k | M \rangle$ constitutes a sum over all length- k nearest-neighbour walks on the line $\{0, 1, \dots, M\}$ that start at M and end at j_* ; each appearance of an oriented edge $e = (\ell \leftrightarrow \ell+1)$ contributes a factor f_j .

Expand $\chi(T)$ in Dyson series and consider again F_h^k . Only $k \geq m$ with $k \equiv m \pmod{2}$ contribute to $\langle j_* | F_h^k | M \rangle$. For any admissible walk of length k from M to j_* , its edge-weight monomial is a product of k factors drawn from $\{f_{\text{int}}, f_{M-1}, f_0\}$. Notice that $f_{M-1}, f_0 \leq C(\delta)$, and the path must cross the boundary edge M at least once. The number of such walks is at most $\binom{k}{(k+m)/2} \leq 2^k$, so

$$|\langle j_* | F_h^k | M \rangle| \leq C(\delta) f_{\text{int}}^k.$$

Hence

$$\left| \frac{(\theta K_{\max} T)^k}{k!} \langle j_* | F_h^k | M \rangle \right| \leq C(\delta) \frac{(\theta K_{\max} T f_{\text{int}})^k}{k!} \leq C(\delta) \left(\frac{e \theta K_{\max} T f_{\text{int}}}{k} \right)^k,$$

using Stirling $k! \geq (k/e)^k$. The rest is the same as the previous Lemmas. \square

Appendix B: Approximation property of the SBP finite difference

In this section, we consider choosing the vector $|r\rangle \propto p^\beta$, with $\beta > 0$. In this case, $\theta F_h |r_h\rangle - |r_h\rangle$ might not be zero at each grid point in the interior. Therefore, we have to take into account such local error in the analysis.

1. Local consistency error

One step in establishing the global accuracy is estimating the local consistency error.

Lemma 8. *Let $v \in C^3[0, 1]$. Define the global constants*

$$M_3 := \left\| v''(p) + \frac{2p}{3} v'''(p) \right\|_{L^\infty(0,1)},$$

Then the following bounds hold,

$$|(F_h v)_i - (Fv)(p_i)| \leq \frac{1}{4} h^2 M_3, \forall 1 \leq i \leq M-1, \quad (\text{B1})$$

Furthermore, if $v(0) = 0$, then $(F_h v)_1 - (Fv)(p_1) = \mathcal{O}(h^2)$; and if $v(0) = v'(0) = 0$, then $(F_h v)_0 - (Fv)(p_0) = \mathcal{O}(h^2)$.

Proof. Using $p_{i\pm 1} = p_i \pm h$ we rewrite the stencil coefficients:

$$\frac{p_{i+1} + p_i}{4h} = \frac{p_i}{2h} + \frac{1}{4}, \quad \frac{p_i + p_{i-1}}{4h} = \frac{p_i}{2h} - \frac{1}{4}.$$

Introduce $A := \frac{p_i}{2h} + \frac{1}{4}$ and $B := \frac{p_i}{2h} - \frac{1}{4}$, so that $A - B = \frac{1}{2}$ and $A + B = \frac{p_i}{h}$.

A Taylor expansion of (A5) about p_i gives

$$\begin{aligned} v(p_{i+1}) &= v(p_i) + h v'(p_i) + \frac{h^2}{2} v''(p_i) + \frac{h^3}{6} v'''(\xi_i), \\ v(p_{i-1}) &= v(p_i) - h v'(p_i) + \frac{h^2}{2} v''(p_i) - \frac{h^3}{6} v'''(\eta_i), \end{aligned}$$

with $\xi_i, \eta_i \in [p_{i-1}, p_{i+1}]$.

Thus, a direct substitution, together with a mean value theorem for the third-order derivatives, yields,

$$\begin{aligned} (F_h v)_i &= (A - B)v(p_i) + h(A + B)v'(p_i) + \frac{h^2}{2}(A - B)v''(p_i) + \frac{h^3}{6}(A + B)v'''(\xi) \\ &= \frac{1}{2}v(p_i) + p_i v'(p_i) + \frac{h^2}{4} v''(p_i) + \frac{p_i h^2}{6} v'''(\xi) \end{aligned}$$

Now we move to the node $i = 1$,

$$(F_h \mathbf{v})_1 = \frac{3}{4}v_2 - \frac{1}{4\sqrt{2}}v_0, \quad p_1 = h.$$

Taylor expand v_2 and v_0 about $p = h$:

$$\begin{aligned} v_2 &= v(h) + hv'(h) + \frac{1}{2}h^2v''(h) + \frac{1}{6}h^3v'''(\xi_2), \\ v_0 &= v(h) - hv'(h) + \frac{1}{2}h^2v''(h) - \frac{1}{6}h^3v'''(\xi_0), \end{aligned} \quad \xi_{0,2} \in (0, 2h).$$

Insert these into the formula and collect like terms:

$$(F_h \mathbf{v})_1 = c_0v(h) + c_1hv'(h) + \frac{c_0}{2}h^2v''(h) + \frac{c_1}{6}h^3v'''(\xi).$$

Here we introduced $c_0 = \frac{3}{4} - \frac{1}{4\sqrt{2}}$, $c_1 = \frac{3}{4} + \frac{1}{4\sqrt{2}}$ and applied the mean value theorem to v''' .

Now the error becomes,

$$\begin{aligned} ((F_h \mathbf{v})_1 - (Fv)(h)) &= (c_0 - \frac{1}{2})v(h) + (c_1 - 1)hv'(h) + \frac{c_0}{2}h^2v''(h) + \frac{c_1}{6}h^3v'''(\xi) \\ &= \frac{1 - 1/\sqrt{2}}{4}[v(h) - hv'(h)] + \frac{c_0}{2}h^2v''(h) + \frac{c_1}{6}h^3v'''(\xi) \\ &= (c_0 - \frac{1}{4})h^2v''(\eta) + \frac{c_1}{6}h^3v'''(\xi). \end{aligned}$$

Here we used a second-order Taylor expansion gives $v(h) - hv'(h) = \frac{1}{2}h^2v''(\eta)$ ($\eta \in (0, h)$).

For the boundary node $i = 0$, $(F\mathbf{v})_0 = \frac{1}{2\sqrt{2}}v(h) = \frac{h^2}{4\sqrt{2}}\theta v''(\zeta)$, again $\mathcal{O}(h^2)$.

Combining the three cases yields the stated bound. \square

Corollary 3. Assume $0 < \theta \leq \frac{2}{7}$. Let

$$\beta = \frac{1}{\theta} - \frac{1}{2}, \quad (\text{B2})$$

$g(p) = p^\beta$. Then, for $1 \leq i \leq M - 1$,

$$\theta |(F_h \mathbf{g})_i - (Fg)(p_i)| \leq C(\theta)h^2p_{i+1}^{\beta-3}, \quad C(\theta) = \frac{\theta}{6}\beta(\beta-1)(\beta-2). \quad (\text{B3})$$

Proof. For $g(p) = p^\beta$ one has $g'''(p) = \beta(\beta-1)(\beta-2)p^{\beta-3}$. Insert this in the exact truncation identity $(F_h \mathbf{g})_i - (Fg)(p_i) = \frac{h^2}{6}p_i g'''(\xi_i)$. Since $\xi_i \in (p_{i-1}, p_{i+1}) \subset [h, 1]$, $\xi_i \leq p_{i+1}$, we get the error bound directly. Since $\beta \geq 3$, the error at the boundary is also $\mathcal{O}(h^2)$ \square

2. Pointwise error at time T

We consider applying the finite difference approximation (A5) with a special class of initial conditions for Eq. (A2),

$$g(p) := \frac{1}{Z_\beta}p^\beta, \quad \beta = \frac{1}{\theta} - \frac{1}{2} > 0, \quad 0 < \theta < 2, \quad (\text{B4})$$

with appropriate values of a to be determined. In particular, we have $Fg = g$, which fulfills the moment conditions. Here we analyze the error due to the approximation of F by (A5).

For the discrete approximation, we choose the following approximation for $|r\rangle$,

$$|r_h\rangle = \sum_{j=0}^M g(p_j) |j\rangle. \quad (\text{B5})$$

The constant Z_β is selected so that,

$$\sum_{j=0}^M g(p_j)^2 = 1.$$

A direct calculation shows that,

$$Z_\beta = \sqrt{\frac{M}{2\beta + 1}} + \mathcal{O}\left(\frac{1}{M}\right). \quad (\text{B6})$$

Let \mathbf{g} be a vector with components $g_i := g(p_i)$ as the grid values. Denote by $u(t, p)$ the solution of Eq. (A1) with initial value in Eq. (B4), and as its approximation, we denote by $\mathbf{u}(t)$ the solution of

$$\dot{\mathbf{u}} = -\kappa(t)\theta F_h \mathbf{u}, \quad \mathbf{u}(0) = \mathbf{g}. \quad (\text{B7})$$

In addition, we impose the exact boundary conditions,

$$u_M(t) = u(t, 1). \quad (\text{B8})$$

To understand how the method might be implemented, we recall the definition of the difference operator F_h (A5), and then write Eq. (B7) in a componentwise form $\forall 2 < i < M$,

$$\dot{u}_i = -\frac{\theta\kappa(t)}{4h} ((p_i + p_{i+1})u_{i+1} - (p_{i-1} + p_i)u_{i-1}). \quad (\text{B9})$$

When $i = M - 1$, the boundary condition (B8) kicks in. Meanwhile, at the left boundary, Eq. (A5) leads to the ODE,

$$\begin{aligned} \dot{u}_1 &= -\theta\kappa(t)\left(\frac{3}{4}u_2 - \frac{1}{4\sqrt{2}}u_0\right) \\ \dot{u}_0 &= -\theta\kappa(t)\frac{1}{2\sqrt{2}}u_1. \end{aligned}$$

Therefore, no boundary condition is needed at the left boundary. This is consistent with the fact that the exact solution propagates to the left. Therefore, the discretization respects the direction of the wave propagation and can be regarded as an upwind scheme.

To derive an error bound, we write the pointwise error $e_i(t) := u_i(t) - u(t, p_i)$. In light of Eq. (B7) and Eq. (B8), we have $e_M(t) = 0$, and $\mathbf{e}(0) = 0$.

Lemma 9 (Error after time T). *The solution of the PDE (A2) with initial value (B4) is given by,*

$$u(t, p) = y(t)g(p),$$

where $\dot{y} = -\kappa(t)y$ and $y(0) = 1$. Assume that $\beta = 1/\theta - 1/2 \geq 3$. Then for every grid point p_i , we have

$$|e_i(T)| \leq C(\theta)Th^2, \quad C(\theta) = \frac{\theta}{6}\beta(\beta - 1)(\beta - 2). \quad (\text{B10})$$

Proof. We prove the first part by direct verification:

$$\frac{d}{dt}y(t)g(p) = -\kappa(t)y(t)g(p) = -\theta\kappa(t)y(t)Fg(p) = -\theta\kappa(t)Fu.$$

Here we have used the fact that $\theta Fg = g$.

To estimate the error, we first subtract the two evolution equations to obtain an error equation,

$$\dot{\mathbf{e}}(t) = -\kappa(t)\theta F_h \mathbf{e}(t) + \boldsymbol{\eta}(t), \quad (\text{B11})$$

where

$$\eta_j(t) := -\theta\kappa(t)(F_h g - Fg)u(t, p_j),$$

is the local consistency error. Corollary 3 gives a time-uniform bound $\|\eta(t)\|_\infty \leq K_{\max}C(\theta)h^2y(t)$, provided that $\beta \geq 3$.

Importantly, since e satisfies the zero boundary condition, from Lemma 4, F_h is skew Hermitian, thus $-\kappa(t)F_h$ in Eq. (B11) generates some unitary operator $U(t, s)$. In addition, the variation of constant formula implies that

$$e(t) = \int_0^t U(t, s)\eta(s)ds.$$

As a result,

$$|e_i(t)| \leq C(\theta)h^2 \int_0^t e^{-\int_0^{t_1} \kappa(t_2)dt_2} dt_1 \leq C(\theta)K_{\max}h^2t.$$

Using $t = T$ yields the claimed estimate. \square

3. Dilation using Eigen-functions p^β with $\beta > 0$

The dilation method based on the differential operator F in Eq. (8) can also use an eigenfunction $|r\rangle \propto p^\beta$ with $\beta > 0$. After the discretization, the residual error $\theta F_h |r_h\rangle - |r_h\rangle$ might not be zero in the interior. Therefore, it generates a local error that needs to be taken into account. Its impact on the final error is summarized in the following theorem.

Theorem 5. *Suppose $\beta \geq 3$ and discretize F by (14) on a uniform grid. Choose θ so that the light-cone condition (22) holds. Then the approximate dilation obeys*

$$\left\| e^{\int_0^T L(s)ds} |\mathbf{x}_0\rangle - (\langle l_h | \otimes I) U_h(T, 0) (|r_h\rangle \otimes |\mathbf{x}_0\rangle) \right\| \leq \frac{C(\theta)X(T)K_{\max}Th^2}{Z_\beta} + \|(\langle i | \otimes I)\chi(T)\|, \quad (\text{B12})$$

where $U_h(T, 0)$ is the unitary generated by the discretized dilated Hamiltonian, $X(T) := \sup_{t \in [0, T]} \|\mathbf{x}(t)\|$, and

$$C(\theta) = \frac{\theta}{6}\beta(\beta-1)(\beta-2), \quad \beta = \frac{1}{\theta} - \frac{1}{2}.$$

In Eqs. (B12) and (22) one sees the trade-off in θ : making θ smaller improves the light-cone margin (delays boundary influence) but increases the bulk prefactor $C(\theta)$; indeed $C(\theta) \sim (6\theta^2)^{-1}$ as $\theta \rightarrow 0$.

Proof. Our goal is to implement the following dilation formula,

$$(I_A \otimes (l|) \mathcal{T} e^{-i \int_0^t \tilde{H}(s)ds} (I_A \otimes |r\rangle) = \mathcal{T} e^{\int_0^t L(s)ds}, \quad \forall t \geq 0, \quad (\text{B13})$$

where,

$$\tilde{H} := I_A \otimes H + iF_\theta \otimes K. \quad (\text{B14})$$

We first present the analysis for a general initial condition $|g\rangle$ is defined in Eq. (B4). For the case when β is an integer, a much easier analysis will be presented in the next section. To connect to the analysis in the preceding sections, we let the exact solution and approximate solution from the dilated dynamics be $|\Psi\rangle$ and $|\Phi\rangle$, respectively. We compare the respective equations as follows,

$$\begin{aligned} \frac{d}{dt} |\Psi(t)\rangle &= -i(I_A \otimes H + iF_\theta \otimes K(t)) |\Psi(t)\rangle, & |\Psi(0)\rangle &= |g\rangle |\mathbf{x}_0\rangle, \\ \frac{d}{dt} |\Phi(t)\rangle &= -i(I_A \otimes H + i\theta F_h \otimes K(t)) |\Phi(t)\rangle, & |\Phi(0)\rangle &= |r_h\rangle |\mathbf{x}_0\rangle. \end{aligned} \quad (\text{B15})$$

Here $|g\rangle$ is defined in Eq. (B4) and $|r_h\rangle$ is the discrete approximation in Eq. (B5) for the consistency with the continuous problem. A similar calculation shows that

$$\Psi(t) = |r_h\rangle \mathcal{T} e^{\int_0^t (-iH(s) + K(s)) ds} |\mathbf{x}_0\rangle,$$

thus encoding the correct solution.

Let us pinpoint the sources of error

1. the discretization of F_θ by θF_h .
2. the zero boundary condition at $p_M = 1$ imposed on χ to ensure the Hermitian property of F_h .

To analyze the sources of the error, we introduce function χ , such that,

$$\frac{d}{dt} |\chi(t)\rangle = -i (I_A \otimes H + i\theta F_h \otimes K(t)) |\chi(t)\rangle, \quad |\chi(0)\rangle = |r_h\rangle |\mathbf{x}_0\rangle, \quad (\text{B16})$$

together the the boundary condition that $(\langle M | \otimes I) \chi(t) = (\langle M | \otimes I) \Psi(t)$.

Therefore, the total error is decomposed into,

$$|\Phi(t)\rangle - |\Psi(t)\rangle = \underbrace{|\chi(t)\rangle - |\Psi(t)\rangle}_{\mathbf{e}(t)} + \underbrace{|\Phi(t)\rangle - |\chi(t)\rangle}_{\mathbf{z}(t)} \quad (\text{B17})$$

First, we observe that the error equation (B11), by extending the definite $\mathbf{e}(t)$ to

$$\mathbf{e}(t) = |\Phi(t)\rangle - |\Psi(t)\rangle,$$

simplify becomes,

$$\dot{\mathbf{e}}(t) = -i (I_A \otimes H + i\theta F_h \otimes K(t)) \mathbf{e}(t) + \boldsymbol{\eta}(t), \quad (\text{B18})$$

where the local truncation error becomes

$$\boldsymbol{\eta}(t) := -\theta (F_h g - F g) \otimes \mathcal{T} e^{\int_0^t (-iH(s) + K(s)) ds} |\mathbf{x}_0\rangle. \quad (\text{B19})$$

Let $Q(T) = \max_{t \in [0, T]} \left\| \mathcal{T} e^{\int_0^t (-iH(s) + K(s)) ds} |\mathbf{x}_0\rangle \right\|$. Using the Hermitian property of F_h and the dissipative condition, we arrive at the same bound that $\|\mathbf{e}(t)\| \leq C(\theta) h^2 Q(T) t$ as in the previous section.

Meanwhile, the other part of the error is,

$$\mathbf{z}(t) = |\Phi(t)\rangle - |\chi(t)\rangle,$$

which satisfies the equation,

$$\frac{d}{dt} \mathbf{z}(t) = -i (I_A \otimes H + \theta F_h \otimes K(t)) \mathbf{z}(t), \quad (\text{B20})$$

with zero initial condition $\mathbf{z}(t) = 0$ while subject to the boundary condition,

$$(\langle M | \otimes I) \mathbf{z}(t) = -\langle M | r_h \rangle \mathcal{T} e^{\int_0^t (-iH(s) + K(s)) ds} |\mathbf{x}_0\rangle. \quad (\text{B21})$$

We note that $\langle M | r_h \rangle = 1/Z_\beta = \mathcal{O}\left(\sqrt{\frac{\beta}{M}}\right)$ from Eq. (B6)

□

Let $H_{\max} = \max_{0 \leq t \leq T} \|H(t)\|$ and $K_{\max} = \max_{0 \leq t \leq T} \|K(t)\|$. Note that K_{\max} is a property of the system and does not scale with M (whereas $\|F_h\| = \Theta(M)$). Combining (B12) with time-dependent interaction-picture simulation [34] gives our first main query bound (with $\tilde{\mathcal{O}}$ hiding polylogarithmic factors).

Theorem 6. *The dilated dynamics can be simulated to precision ϵ using*

$$\tilde{\mathcal{O}} \left(TH_{\max} + \frac{X(T)^{1/2} T^{3/2} K_{\max}}{\epsilon^{1/2}} \right)$$

block-encoding queries to the oracles for $H(t)$ and $K(t)$.

The $\sqrt{T/\epsilon}$ in the second term reflects the second-order truncation error in (14). When $K_{\max} \ll H_{\max}$, this already yields reasonable complexity. A remaining subtlety is the postselection success probability. With the weighted discretization

$$|r_h\rangle = Z_{\beta}^{-1} \sum_{j=0}^M p_j^{\beta} w_j^{1/2} |j\rangle, \quad Z_{\beta}^2 = \sum_{j=0}^M w_j p_j^{2\beta} \approx \int_0^1 p^{2\beta} dp = \frac{1}{2\beta + 1},$$

postselecting a single site $p_* = p_i$ on a uniform grid ($w_i \approx 1/M$) gives

$$P_{\text{succ}} = |\langle i | r_h \rangle|^2 \approx \frac{(2\beta + 1)p_*^{2\beta}}{M}. \quad (\text{B22})$$

Thus when $K_{\max}T \gg 1$ (stiff regimes) and β is large, the success probability for a fixed site can become exponentially small in β ; in practice one should choose j_* in the interior (or aggregate several sites) to maintain a reasonable postselection rate.